NEURODEGENERATIVE DISEASES

Treatment of a genetic brain disease by CNS-wide microglia replacement

Yohei Shibuya[1,2], Kevin K. Kumar[1,3]†, Marius Marc-Daniel Mader[1,2]†, Yongjin Yoo[1,2]†, Luis Angel Ayala[1,2], Mu Zhou[4], Manuel Alexander Mohr[5], Gernot Neumayer[1,2], Ishan Kumar[1,2], Ryo Yamamoto[1,6], Paul Marcoux[1,2], Benjamin Liou[7], F. Chris Bennett[8], Hiromitsu Nakauchi[1,6,9], Ying Sun[7,10], Xiaoke Chen[5], Frank L. Heppner[11,12,13,14,15], Tony Wyss-Coray[16,17], Thomas C. Südhof[4,18], Marius Wernig[1,2]*‡

Hematopoietic cell transplantation after myeloablative conditioning has been used to treat various genetic metabolic syndromes but is largely ineffective in diseases affecting the brain presumably due to poor and variable myeloid cell incorporation into the central nervous system. Here, we developed and characterized a near-complete and homogeneous replacement of microglia with bone marrow cells in mice without the need for genetic manipulation of donor or host. The high chimerism resulted from a competitive advantage of scarce donor cells during microglia repopulation rather than enhanced recruitment from the periphery. Hematopoietic stem cells, but not immediate myeloid or monocyte progenitor cells, contained full microglia replacement potency equivalent to whole bone marrow. To explore its therapeutic potential, we applied microglia replacement to a mouse model for Prosaposin deficiency, which is characterized by a progressive neurodegeneration phenotype. We found a reduction of cerebellar neurodegeneration and gliosis in treated brains, improvement of motor and balance impairment, and life span extension even with treatment started in young adulthood. This proof-of-concept study suggests that efficient microglia replacement may have therapeutic efficacy for a variety of neurological diseases.

INTRODUCTION

Rectifying disease pathology in the nervous system remains one of the grand challenges in medicine. In principle, neural cell therapies are an attractive approach because a one-time treatment has the potential to have long-lasting effects. Although local grafts are highly promising, such as cell transplantation for Parkinson's disease (*1*, *2*), the large size of the human brain and the need for stereotactic injection complicate the homogeneous distribution of grafted cells even when highly migratory cells like oligodendrocyte precursors are transplanted (*3*). Thus, alternative approaches are needed to achieve more homogeneous brain incorporation, preferably delivered via the circulation.

Hematopoietic cell transplantation (HCT) is a widely used therapeutic procedure to replace a patient's hematopoietic system (*4*). In addition to diseases of the bone marrow, allogeneic HCT has been used to treat systemic genetic syndromes (*5*, *6*).

The widespread distribution of hematopoietic cells and their continued turnover and replacement from bone marrow stem cells allow body-wide delivery of a functional gene product. For instance, decades of experience have shown that HCT can rescue many pathological aspects in children with severe forms of genetic metabolic syndromes (*7*). However, central nervous system (CNS) involvement and resulting pathology have limited response to HCT presumably due to the inefficient replacement of brain-resident microglia by the bone marrow (*5*, *6*, *8*). Unlike other tissue-resident macrophages, microglia are long-lived and regenerated from within the brain (*9*–*13*). Moreover, peripheral administration of therapeutic gene products has limited efficacy as large molecules are unable to efficiently traverse the blood-brain barrier (BBB) (*14*, *15*). Thus, cellular or molecular access to the brain is urgently needed to efficiently treat such genetic CNS diseases.

Here, we and others recently developed a rapid and near-complete replacement of microglia in mice with circulation-derived myeloid cells (CDMCs) eliminating the large variability observed after conventional bone marrow transplantation (BMT) (*16*, *17*). These findings beg the question whether such widespread microglia replacement may be a potential solution for the unmet clinical need to effectively treat genetic brain diseases and reliably deliver therapeutic proteins into the CNS.

[1]Institute for Stem Cell Biology and Regenerative Medicine and Department of Pathology, Stanford University School of Medicine, Stanford, CA 94305, USA. [2]Department of Pathology, Stanford University School of Medicine, Stanford, CA 94305, USA. [3]Department of Neurosurgery, Stanford University School of Medicine, Stanford, CA 94305, USA. [4]Department of Molecular and Cellular Physiology, Stanford University School of Medicine, Stanford, CA 94305, USA. [5]Department of Biology, Stanford University, Stanford, CA 94305, USA. [6]Department of Genetics, Stanford University School of Medicine, Stanford, CA 94305, USA. [7]Division of Human Genetics, Cincinnati Children's Hospital Medical Center, Cincinnati, OH 45229, USA. [8]Department of Psychiatry, Perelman School of Medicine, University of Pennsylvania, Philadelphia, PA 19104, USA. [9]Division of Stem Cell Therapy, Distinguished Professor Unit, The Institute of Medical Science, The University of Tokyo, Tokyo 108-8639, Japan. [10]Department of Pediatrics, University of Cincinnati College of Medicine, Cincinnati, OH 45229, USA. [11]Department of Neuropathology, Cluster of Excellence, NeuroCure, Charité–Universitätsmedizin Berlin, 10117 Berlin, Germany. [12]Department of Neuropathology, Charité–Universitätsmedizin Berlin, corporate member of Freie Universität Berlin, Humboldt-Universität zu Berlin, and Berlin Institute of Health, 10117 Berlin, Germany. [13]Cluster of Excellence, NeuroCure, Charitéplatz 1, 10117 Berlin, Germany. [14]Berlin Institute of Health (BIH), 10117 Berlin, Germany. [15]German Center for Neurodegenerative Diseases (DZNE) Berlin, 10117 Berlin, Germany. [16]Department of Neurology and Neurological Sciences, Stanford University School of Medicine, Stanford, CA 94305, USA. [17]Veterans Administration Palo Alto Healthcare System, Palo Alto, CA 94304, USA. [18]Howard Hughes Medical Institute, Stanford University School of Medicine, Stanford, CA 94305, USA.
*Corresponding author. Email: wernig@stanford.edu
†These authors contributed equally to this work.
‡Lead contact.

RESULTS

Microglia replacement after BMT is slow, inefficient, and highly variable

The reported efficiencies of microglia replacement after BMT in mice vary greatly (*18*–*23*). We therefore first sought to systematically characterize this process and performed BMT using green fluorescent protein (GFP)–transgenic donor cells and busulfan to precondition the bone marrow (Fig. 1A). The engraftment of GFP$^+$ CDMCs into the brain was not synchronized and occurred much later than GFP chimerism in the peripheral blood (Fig. 1, B and C). Only after 12 weeks, most cells adopted a microglia-like ramified morphology (Fig. 1, D and E). The degree of brain chimerism was highly variable between mice ranging from 7.1 to 73.4% (Fig. 1C). Unlike in the blood, the degree of chimerism plateaued in the brain and did not significantly increase further even 6 months after transplantation (12 weeks versus 24 weeks, $P = 0.99$; Fig. 1C).

The mechanisms how cells from the circulation can enter the brain are unclear. Genetic depletion of microglia enables incorporation of various hematopoietic cells into the brain (*24*), but similarly efficient pharmacological microglia depletion does not (*11*, *25*). To

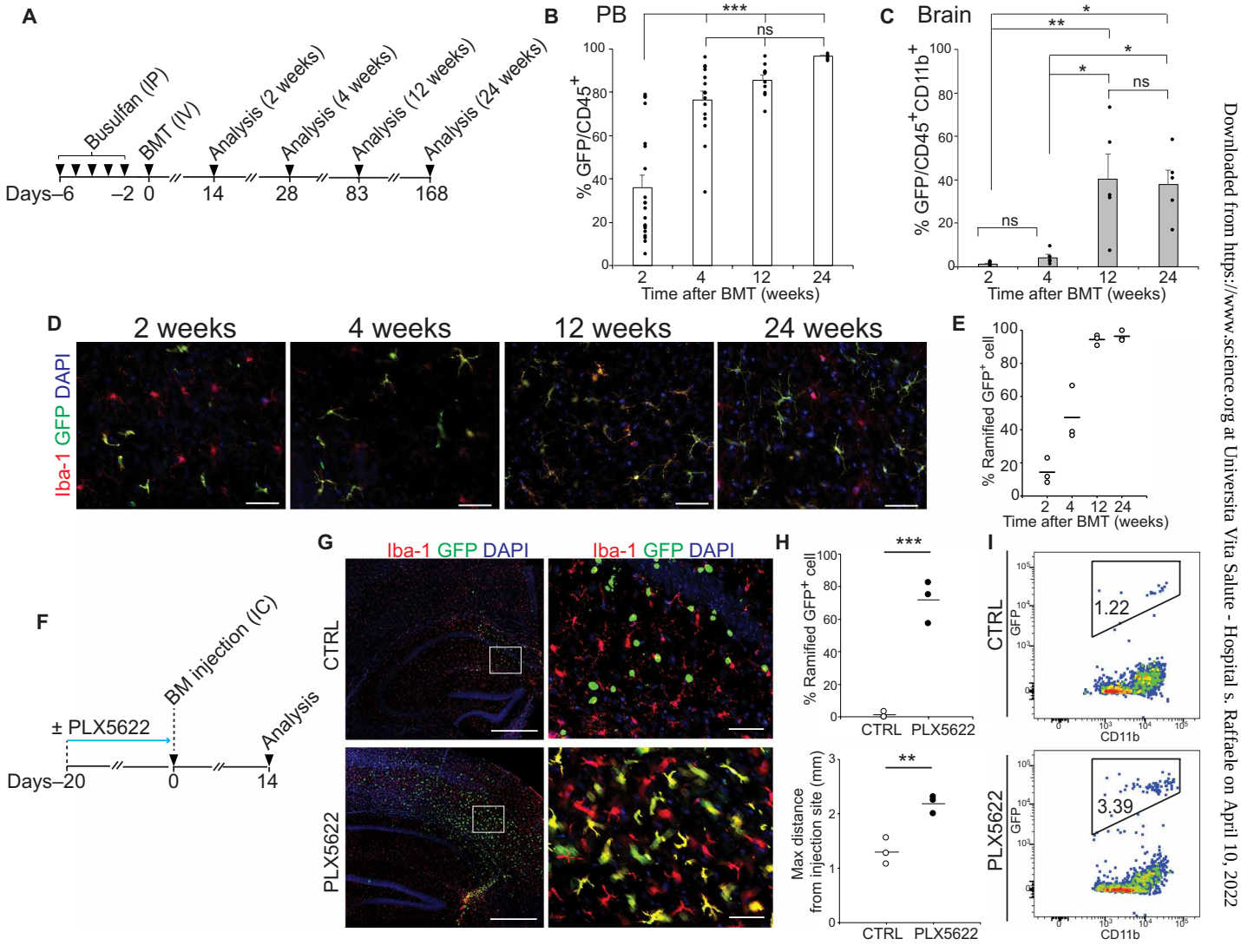

Fig. 1. Microglia replacement after bone marrow transplantation is a slow, inefficient, and variable process. (**A**) Schematic overview of bone marrow transplantation (BMT). IP, intraperitoneal; IV, intravenous. (**B** and **C**) Flow cytometry analysis of donor chimerism in peripheral blood (PB) leukocytes (CD45$^+$ cells) and brain myeloid cells (CD45$^+$CD11b$^+$ cells) at the indicated time point. GFP chimerism in PB leukocytes (B) (mean ± SEM, $n = 5$ to 20 per time point; ***$P < 0.001$; ns, not significant, ANOVA). GFP chimerism in brain myeloid cells (C) (mean ± SEM, $n = 5$ per time point; *$P < 0.05$ and **$P < 0.01$, ANOVA). (**D**) Representative images of circulation-derived myeloid cells (CDMCs) (Iba-1$^+$GFP$^-$) and host microglia (Iba-1$^+$GFP$^-$) cells and 4′,6-diamidino-2-phenylindole (DAPI) in the cortex of recipient mice at the indicated time points. Scale bars, 50 mm. (**E**) Percentage of ramified GFP$^+$ cells at the indicated time points ($n = 3$ per time point, three brain slices per animal were quantified). (**F**) Schematic overview of direct intracerebral (IC) injection of GFP$^+$ BMCs with or without PLX5622 pretreatment of recipient mice. (**G**) Representative images of GFP$^+$ and Iba-1$^+$ cells and DAPI in the brain 14 days after IC injection. The right panels are enlarged images of the boxed areas in the left panels. Scale bars, 500 μm (left) and 50 μm (right). CTRL, control. (**H**) Quantification of transplanted GFP$^+$ BMCs in coronal brain sections. Top: Percentage of ramified GFP$^+$ cells. Bottom: Maximum migration distance of GFP$^+$ cells from the injection site. Horizontal bars represent mean values ($n = 3$ per group, three brain slices per animal were quantified; **$P < 0.01$ and ***$P < 0.001$, Student's t test). (**I**) Flow cytometry analysis of GFP$^+$ BMCs 14 days after direct intracerebral IC injection with (bottom) and without (top) PLX5622 pretreatment of recipient mice.

specifically address the direct effects of microglial niche factors on hematopoietic cells, we injected GFP-labeled, unpurified bone marrow cells (BMCs) directly into the hippocampus of mice with or without a 21-day pretreatment of PLX5622 (Fig. 1F), a potent CSF1R inhibitor (*26*). BMCs injected into control brains survived for 2 weeks but retained a round morphology, and no grafted cell expressed the microglial marker Iba-1 (Fig. 1G). In contrast, most BMCs injected into PLX5622-treated, microglia-depleted mice exhibited ramified morphologies; almost all expressed Iba-1, were more numerous, and had migrated further from the injection site (Fig. 1, G to I). In the same time frame, intravenously injected donor cells did not display similar microglial differentiation after BMT (Fig. 1, D and E). In consistent with a previous report (*17*), these data demonstrate that elimination of endogenous microglia is critically required for BMCs to engraft in the brain and differentiate into microglia-like cells.

Microglia depletion after BMT results in near-complete replacement of microglia with CDMCs throughout the entire brain

We next sought to engage microglial niche factors during BMT. CSF1R inhibition before BMT did not affect incorporation of CDMCs. However, mice transiently treated with PLX5622 4 weeks after BMT consistently exhibited over 90% GFP^+ cells among all brain myeloid cells by flow cytometry (Fig. 2, A to C). Histological analysis revealed that the vast majority of GFP^+ cells had a microglia-like morphology and stained for Iba-1 in multiple brain regions (Fig. 2D and fig. S1A) and had homogeneously populated the entire brain and spinal cord (Fig. 2, E and F, and fig. S1, B and C). CDMCs remained stably incorporated for at least 6 months after transplantation (Fig. 2C and fig. S1A). As seen in native mice (*27*), PLX5622 treatment after BMT had no major effects on various monocyte populations in the peripheral blood (fig. S1, D and E). As reported for conventional BMT (*16*) and also in our method, we found donor-derived myeloid cells in the choroid plexus, meninges, and perivascular region (fig. S2A). GFP chimerism in tissue-resident macrophages in the skin, lung, and liver was not further increased over BMT only (fig. S2, B and C).

CDMCs and microglia are transcriptionally distinct cells

To molecularly characterize incorporated CDMCs, we purified CDMCs after our high-efficiency replacement BMT followed by PLX5622 treatment [CDMC (BMT + P)], CDMCs after BMT only [CDMC (BMT only)] 3 months after transplantation, and age-matched endogenous microglia by fluorescence-activated cell sorting (FACS) and performed RNA sequencing (RNA-seq) in these cells. Principal components analysis (PCA) and unbiased hierarchical clustering showed that CDMC (BMT + P), CDMC (BMT only), and microglia have distinct gene expression profiles (Fig. 3, A and B). A recent study generated gene expression profiles of microglia-like cells engrafted into the brain derived from many different hematopoietic cell populations (*24*). Unbiased hierarchical clustering showed that our microglia samples (green open triangles) clustered together with the published microglia populations, our cell population after BMT only (open yellow triangles) clustered with the published BMT cells, and CDMCs after BMT + P (purple open triangles) formed a distinct group that also contained fetal liver-derived microglia-like cells (Fig. 3C). *Ms4a7* and *Clec12a* are markers of periphery-derived brain macrophages but are lowly expressed in microglia (*24*). Quantitative real-time polymerase chain reaction (PCR) analysis revealed that *Ms4a7* and *Clec12a* transcripts were higher in CDMC (BMT + P) than in microglia but lower than in CDMC (BMT only) (Fig. 3D). A direct comparison between CDMCs and microglia revealed 1296 differentially expressed genes ($\log_2$ fold change > 1 and false discovery rate < 0.05) between microglia (564) and CDMCs (732) (fig. S3A), reminiscent of previously published datasets using genetic approaches to replace microglia (fig. S3, B and C) (*28*, *29*). The PCA plot showed that CDMCs remained transcriptionally distinct from microglia 8 and 10 months after BMT (fig. S3D). Microglia play crucial roles in synaptic pruning, scavenging activity, antigen processing and presenting, and cytokine-mediated immunity in the CNS (*30*, *31*). We selected lists of genes involved in these microglia functions based on gene ontology terms and analyzed expression of the genes in microglia and CDMCs by RNA-seq. The heatmaps showed distinct expression patterns of these genes in microglia and CDMCs (fig. S4A), suggesting that CDMCs may function differently from microglia. Recently, microglia with similar pathological features termed disease-associated microglia (DAM) or microglial neurodegenerative (MGnD) phenotypes were identified in various disease states including Alzheimer's disease, amyotrophic lateral sclerosis, tauopathies, multiple sclerosis, and aging (*32*–*35*). In DAM, a specific subset of genes termed DAM genes is up-regulated, whereas microglia homeostatic genes are down-regulated (*32*, *33*). Similar to DAM, CDMCs after our BMT + P method showed increased expression of DAM genes such as *Apoe*, *Cd63*, *Ctsb*, and *Spp1* and decreased expression of microglia homeostatic genes such as *Gpr34*, *P2ry12*, *Sall1*, and *Tmem119* (fig. S4B). These RNA-seq data suggest that CDMCs are transcriptionally distinct from microglia even long term after transplantation, and gene expression profile of CDMCs is similar to DAM, which is in consistent with previous studies using various transplantation systems (*24*, *28*, *29*).

Flow cytometry analysis revealed that CDMCs after conventional BMT only had slightly higher expression of CD45 and slightly lower expression of CD11b than microglia (Fig. 3E). Using these two surface markers, CDMC (BMT + P) moved closer toward microglia over time (Fig. 3E). Unlike CDMCs after BMT only, we found robust expression of the microglia-specific marker TMEM119 (*36*) in CDMCs after BMT + P (48.3% versus 87.6%, $P < 0.001$; Fig. 3F). Thus, CDMCs are transcriptionally distinct from microglia, and transient CSF1R inhibition not only increases the efficiency of CDMC incorporation by BMT but also affects the transcriptional state of CDMCs.

CDMCs incorporated into the brain have a distinct morphological and functional state from microglia

We next performed a detailed morphometric characterization of CDMCs at 12 and 24 weeks after transplantation. Whereas CDMCs after BMT + P rapidly adopted a ramified microglia-like morphology shortly after PLX5622 withdrawal (fig. S5), their processes were thicker, shorter, and less branched at 12 weeks after transplantation (Fig. 4, A and B), reminiscent of activated microglia (*37*). The number of branched processes increased over time but was still significantly lower ($P < 0.001$) than microglia at 24 weeks after transplantation. Another notable difference was that the density of CDMCs was higher than endogenous microglia at both time points (Fig. 4, A and B).

In the next set of experiments, we assessed functional properties of CDMCs in comparison to microglia. Freshly isolated CDMCs were able to phagocytose beads in vitro at a rate higher than microglia

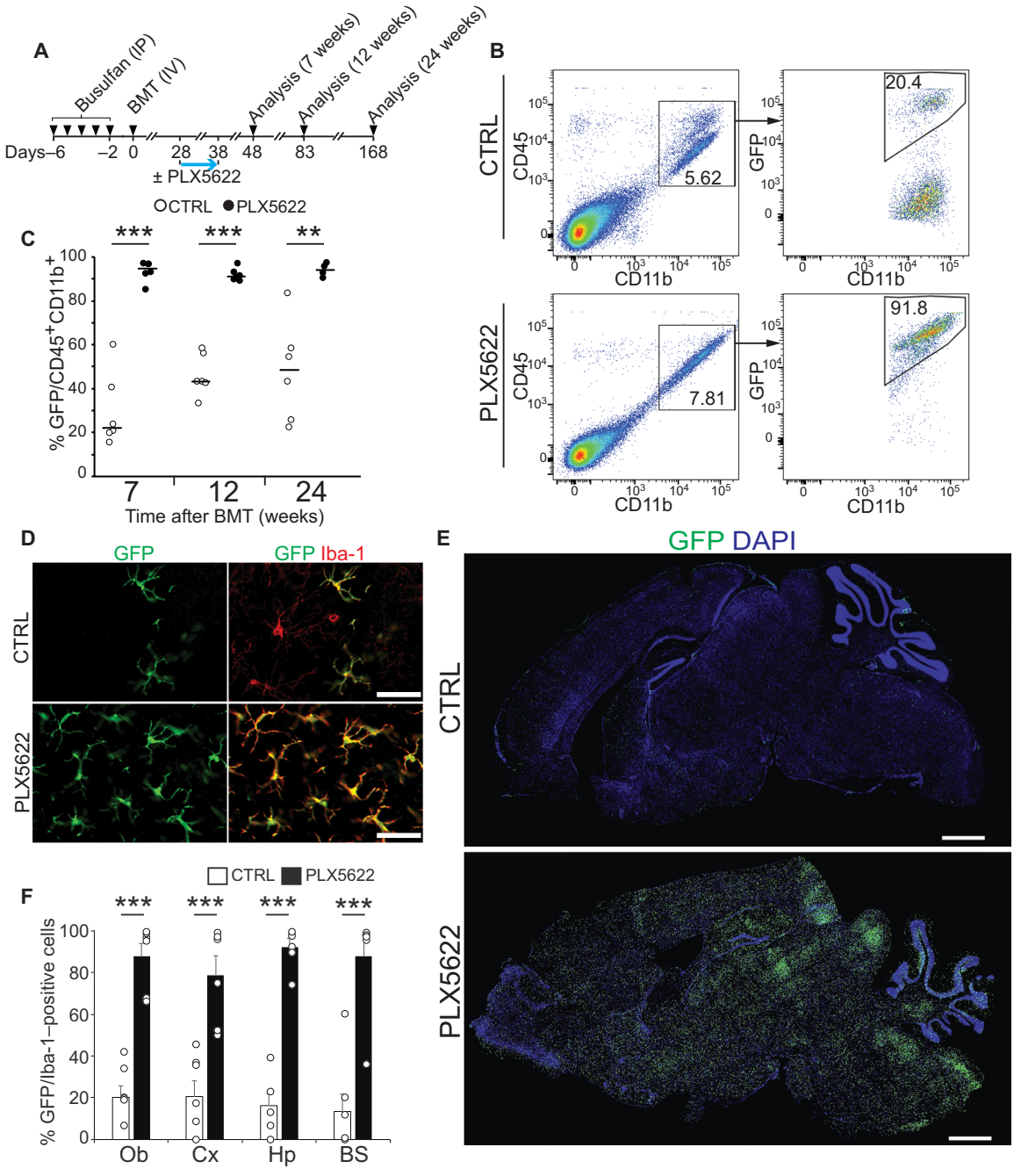

Fig. 2. A transient treatment with PLX5622 after BMT results in efficient and stable donor myeloid chimerism in the brain. (**A**) Schematic overview of BMT with PLX5622 treatment. Recipient mice were treated with PLX5622 or vehicle control (CTRL) for 10 days starting on day 28. Donor chimerism was analyzed at the indicated time points. (**B**) Flow cytometry gating for analysis of myeloid chimerism in the brain. (**C**) Myeloid chimerism in the brain was analyzed by flow cytometry at the indicated time points (horizontal bars represent median values, $n = 5$ to 6 per time point; $^{**}P < 0.01$ and $^{***}P < 0.001$, Student's t test). (**D**) Representative images of GFP$^+$ and Iba-1$^+$ cells in the cortex on day 83. Scale bars, 50 μm. (**E**) Sagittal brain sections showing GFP$^+$ cells and DAPI on day 83. Scale bars, 1 mm. (**F**) Quantification of GFP$^+$ and Iba-1$^+$ cells in the indicated brain regions on day 83. Ob, olfactory bulb; Cx, cortex; Hp, hippocampus; BS, brain stem (mean ± SEM, $n = 6$ per group, three brain sections per animal were quantified; $^{***}P < 0.001$, Student's t test).

(Fig. 4, C and D). Accordingly, they had higher expression of the endolysosomal marker CD68 in situ (fig. S6, A to C). Using two-photon live microscopy, we observed that CDMCs at 12 weeks after transplantation were highly dynamic, continuously extending and retracting their processes, a known microglial property (Fig. 4, E and F, and movies S1 and S2) (*38*, *39*). Process tracking and quantification revealed that CDMCs displayed a slight increase in motility compared to microglia (Fig. 4G). To assess their immunological response to pathogenic stimuli, we systemically injected phosphate-buffered saline (PBS) or lipopolysaccharide (LPS) into mice with or without

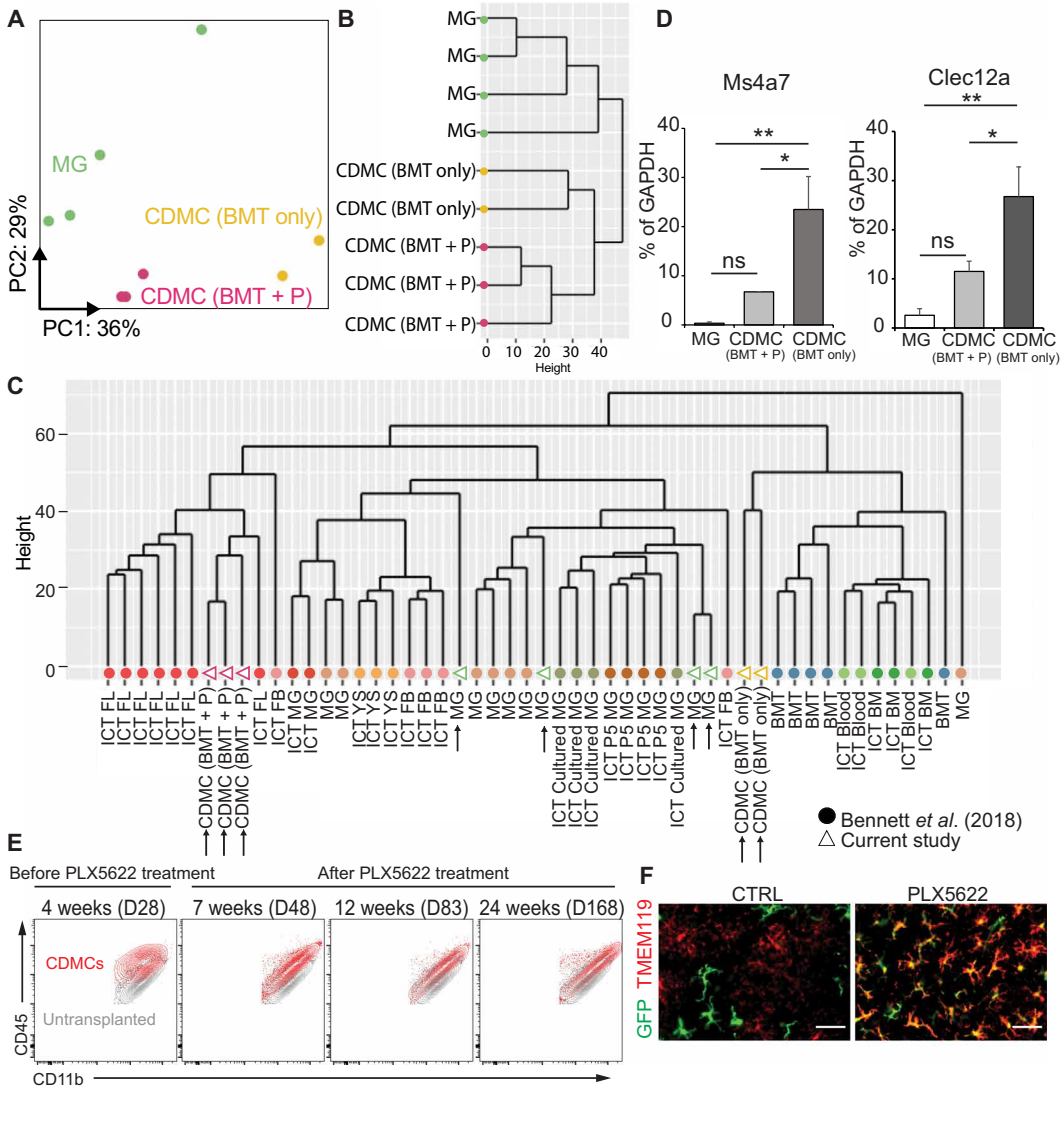

Fig. 3. CDMCs and microglia are transcriptionally distinct cells. (**A**) Principal components analysis (PCA) plot for microglia ($n = 4$, green), CDMC (BMT + P) ($n = 3$, purple), and CDMC (BMT only) ($n = 2$, yellow) using 2500 most variable genes. Ellipses demarcate 95% confidence interval for assigned clusters. (**B**) Unsupervised hierarchical clustering of microglia, CDMC (BMT + P), and CDMC (BMT only). (**C**) Unsupervised hierarchical clustering of our dataset and a published dataset of various microglia-like cells of different origins (*24*). Our samples are shown as open triangles, and the published data are shown as filled circles. CDMC after BMT with PLX5622 treatment [CDMC (BMT + P)], CDMC after conventional BMT without PLX5622 treatment [CDMC (BMT only)], microglia (MG), intracranial transplanted (ICT)–P5 microglia (ICT P5 MG), ICT-cultured microglia (ICT Cultured MG), ICT-adult microglia (ICT MG), ICT–yolk sac cells (ICT YS), ICT–fetal brain cells FB (ICT FB), ICT–fetal liver cells (ICT FL), ICT-BM cells (ICT BM), ICT-PB (ICT Blood), and bone marrow transplanted by IP (BMT). (**D**) Quantitative real-time PCR analysis of bone marrow–derived microglia-like cell marker *Ms4a7* and *Clec12a* in microglia and CDMCs (mean ± SEM, $n = 6$; $^*P < 0.05$ and $^{**}P < 0.01$, ANOVA). GAPDH, glyceraldehyde-3-phosphate dehydrogenase. (**E**) Overlaid density plots of CDMCs (red) of BMT + PLX5622 protocol (BMT + P) at the indicated time points and myeloid cells of untransplanted mice (gray). (**F**) Representative images of GFP$^+$ and TMEM119$^+$ cells in the cortex on day 83 (D83). Scale bars, 50 μm.

BMT + P at 12 weeks after transplantation and then measured a panel of cytokines in the brain by a multiplex bead–based assay 24 hours after LPS injection. Without LPS stimulation, 5 of 38 cytokines [Eotaxin, vascular endothelial growth factor (VEGF), leukemia inhibitory factor (LIF), interleukin-3 (IL-3), and IL-13] examined were differentially produced in the brains between CDMC-containing and normal mice; however, the relative response of all cytokines in the brain to LPS stimulation was comparable between two groups (table S1). Last, we determined the effects of CDMC incorporation on overall brain function 12 weeks after BMT + P. The Y-maze test showed that CDMC-bearing mice had no spatial working memory deficiency (fig. S6, D and E).

High CDMC brain chimerism is best explained by the proliferative advantage of surviving CDMCs during PLX5622 withdrawal rather than continued influx from peripheral circulation

We next sought to better understand how the transient CSF1R blockade results in the robust CDMC incorporation at the expense of microglia. First, we hypothesized that CDMCs might be less sensitive to CSF1R inhibition, which would lead to a selective survival advantage during the PLX5622 treatment. CDMCs had less surface CSF1R expression than microglia (Fig. 5A). However, we found that both CDMCs and microglia disappeared during PLX5622 treatment (Fig. 5B, blue arrow). Only after withdrawal of PLX5622, CDMCs rapidly took over in numbers (Fig. 5B, after day 41).

To explore whether the high CDMC chimerism is due to increased cell recruitment from the circulation, we performed a lineage tracing experiment. We succeeded to genetically label CDMCs and peripheral blood cells with different fluorescent proteins using the following approach: First, we transplanted bone marrow from Cx3cr1::CreER; Rosa26::loxStoplox::tdTomato; Ubc::EGFP mice to wild-type (WT) mice using our BMT + P method (Fig. 5C and fig. S7A). Thus, all donor cells constitutively expressed GFP, and upon tamoxifen injection, all donor-derived CX3CR1$^+$ myeloid cells expressed tdTomato (fig. S7B). Because peripheral blood myeloid cells are short-lived (*40*) and hematopoietic stem cells (HSCs) are CX3CR1 negative, over time, recombined tdTomato-positive cells in blood

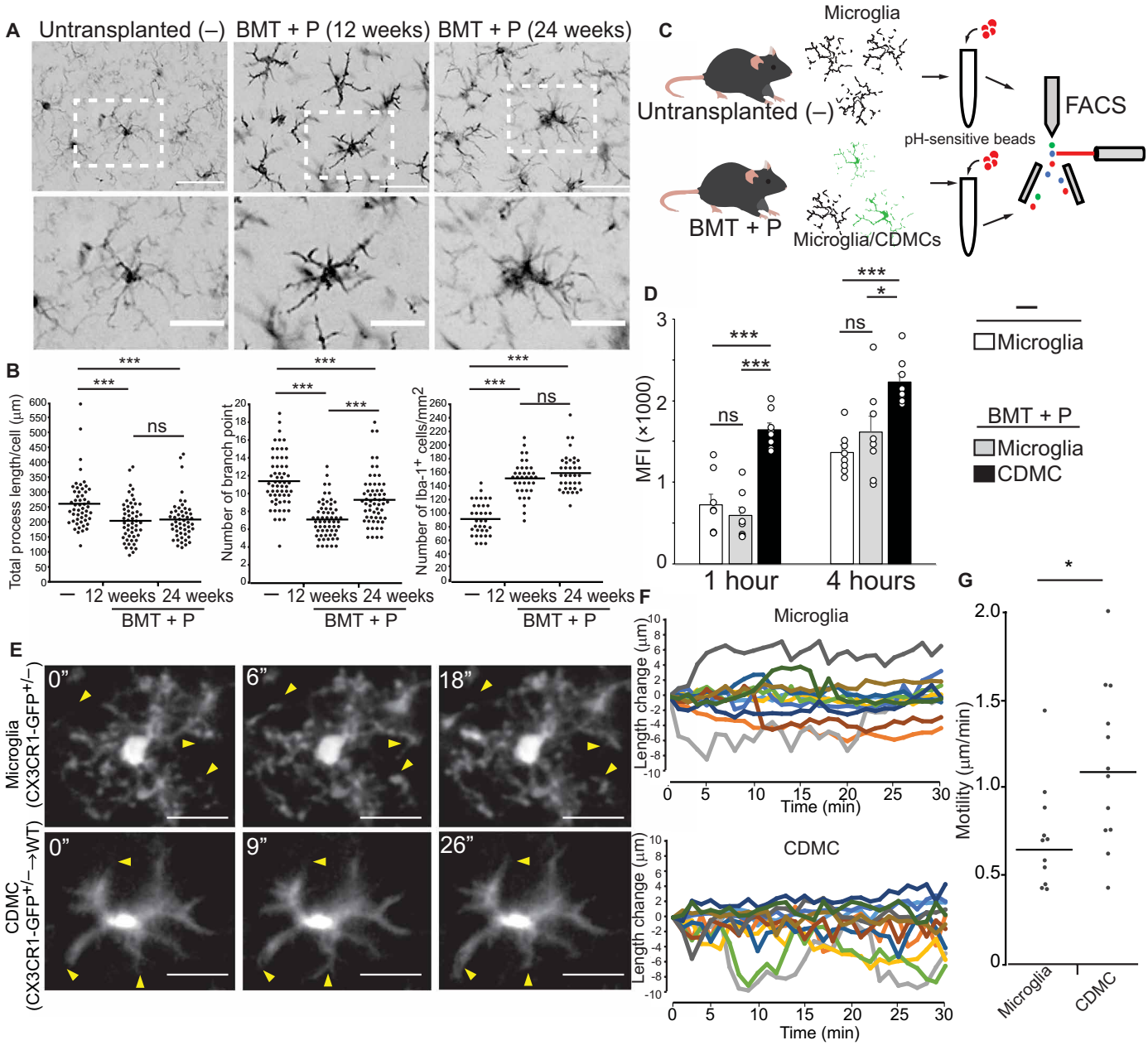

Fig. 4. CDMCs are morphologically and functionally similar but distinct from microglia. (**A**) Representative images of Iba-1$^+$ cells in the cortex of untransplanted mice (–), mice after BMT + P (12 weeks after transplantation), and mice after BMT + P (24 weeks after transplantation). The bottom panels are enlarged images of the boxed areas in the top panels. Scale bars, 50 μm (top) and 25 μm (bottom). (**B**) Quantitative, morphological analysis of Iba-1$^+$ in the indicated samples. Left: Total length of processes. Middle: Number of branch points. Right: Cell density (horizontal bars represent median values, $n = 3$ per group, three brain slices per animal were quantified; ***$P < 0.001$, ANOVA). (**C**) Schematic overview of in vitro phagocytosis assay of brain myeloid cells. Phagocytosis of pH-sensitive fluorescent beads was analyzed by flow cytometry. (**D**) Mean fluorescence intensity (MFI) of pH-sensitive fluorescent beads in the indicated samples 1 and 4 hours of incubation (mean ± SEM, $n = 8$; *$P < 0.05$ and ***$P < 0.001$, ANOVA). (**E**) Microglia (CX3CR1-GFP$^{+/-}$) and CDMCs (CX3CR1-GFP$^{+/-}$→WT) were visualized in vivo by two-photon microscopy. Individual frames from 30-min time-lapse imaging of microglia (top) and CDMCs (bottom). Representative images are shown. Arrowheads indicate extension and retraction of processes. Scale bars, 25 μm. (**F**) Changes in process length were analyzed in eight cells per group (total of 12 processes per group). Images were taken every 1 min for 30 min. (**G**) Motility of processes in microglia and CDMCs (horizontal bars represent median values, $n = 12$ processes per group; *$P < 0.05$, Student's t test).

should be replaced with GFP only–expressing cells. In contrast, if CDMCs were long-lived and not replaced by HSCs as microglia (*13*), they should remain tdTomato$^+$ and GFP$^+$ over time (fig. S7C). Flow cytometry analysis of transplanted mice demonstrated that this prediction was correct: Fig. 5D shows that the fraction of tdTomato$^+$ myeloid cells in the peripheral blood decreased over time and was undetectable 35 days after tamoxifen injection. Brain CDMCs, on the other hand, were labeled at around 80% for at least 84 days (Fig. 5, D and E). Thus, we have created mice in which brain CDMCs were tdTomato$^+$GFP$^+$ and peripheral blood cells were

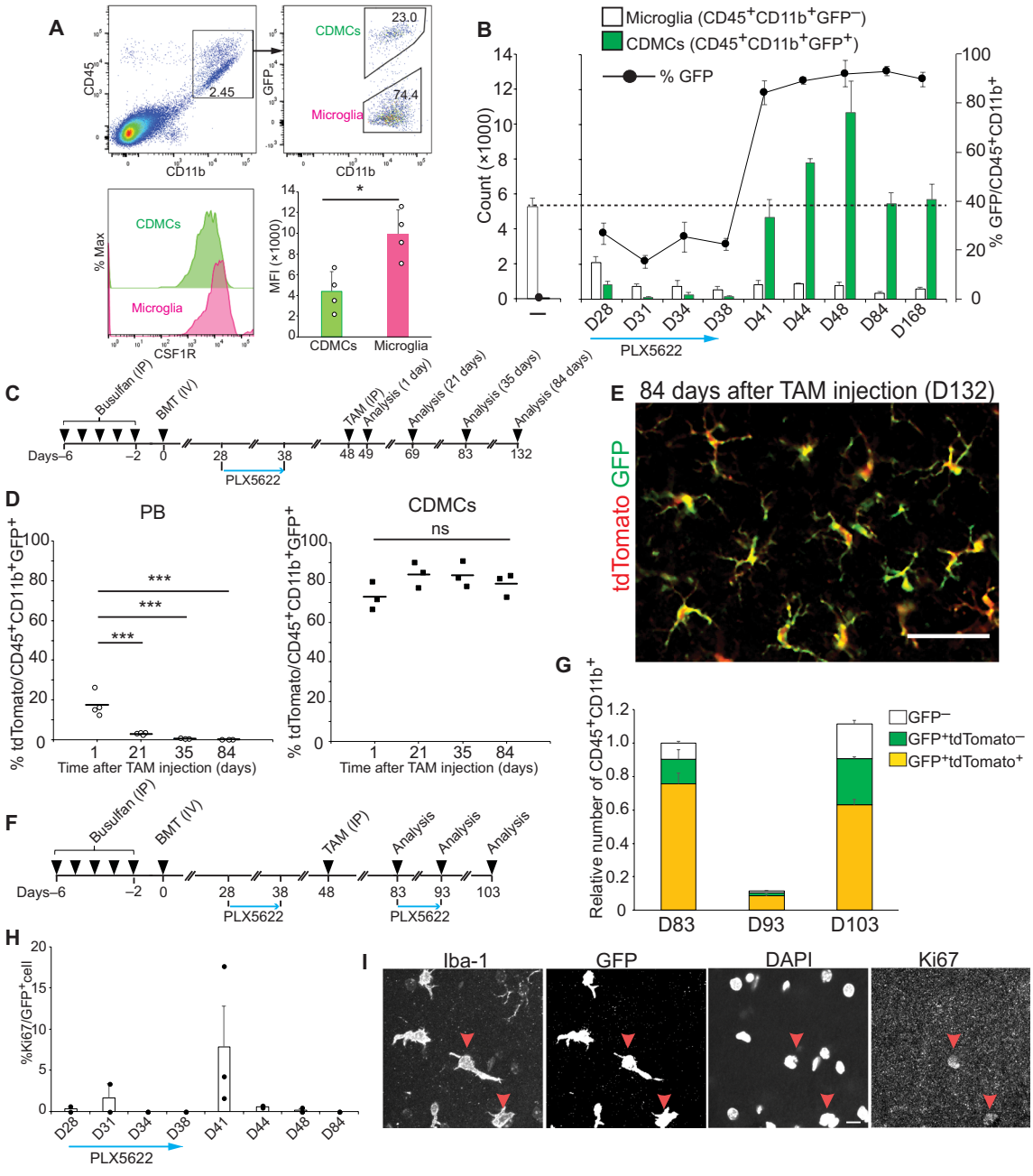

Fig. 5. Efficiently engrafted CDMCs are primarily derived from expanded residual cells rather than from continued influx. (**A**) Flow cytometry analysis of expression of CSF1R in CDMCs and microglia on day 28 (mean ± SEM, $n = 4$ per group; $^*P < 0.05$, Student's t test). (**B**) Time-course analysis of $CD45^+CD11b^+GFP^-$ (endogenous microglia) and $CD45^+CD11b^+GFP^+$ cells (CDMCs) after BMT during and after PLX5622 treatment. The number of the indicated cell populations was analyzed by flow cytometry ($n = 3$ to 4 per time point). (**C**) Schematic of the BMT + P experimental protocol. (**D**) Expression of tdTomato in GFP^+ myeloid cells in PB and the brain (CDMCs) was analyzed by flow cytometry at the indicated time point (horizontal bars represent mean values; $n = 3$ per time point; $^{***}P < 0.001$, ANOVA). (**E**) Representative images of GFP^+ and $tdTomato^+$ cells in the cortex on day 132, i.e., 84 days after tamoxifen injection. Scale bars, 50 μm. (**F**) Schematic of BMT with PLX5622 to study repopulation of CDMCs after acute depletion. (**G**) Expression of GFP and tdTomato in brain myeloid cells was analyzed by flow cytometry at the indicated time points ($n = 3$ per time point). (**H**) $Ki67^+GFP^+$ cells in the brain were quantified using immunofluorescence microscopy during and after PLX5622 treatment ($n = 2$ to 3 per time point). (**I**) Representative images of Iba-1^+, GFP^+, $Ki67^+$ cells and DAPI on day 41. Red arrowheads indicate $Ki67^+$ cells. Scale bars, 10 μm.

$tdTomato^-GFP^+$. These mice were then treated with a second round of PLX5622 for 10 days (Fig. 5F). Flow cytometry analysis demonstrated that after repopulation again, most brain myeloid cells were $tdTomato^+$, demonstrating that most CDMCs are derived from preexisting brain-resident CDMCs and not from the peripheral blood (Fig. 5G and fig. S7D). Thus, the high CDMC chimerism is caused by a competitive growth advantage of CDMCs over endogenous microglia after PLX5622 withdrawal. This conclusion is further corroborated by our finding that CDMCs are usually quiescent but become proliferative right after PLX5622 withdrawal (Fig. 5, H and I).

Injection of purified HSCs results in high-efficiency microglia repopulation

Whole bone marrow (WBM) is heterogeneous and ill-defined. We therefore sought to evaluate which specific hematopoietic cell population had the highest capacity of generating CDMC engraftment in our BMT + P protocol. To this end, we purified eight hematopoietic cell types (*41*) and injected 12,500 cells of each cell type as well as the same number of WBM as positive control into busulfan-conditioned mice (Fig. 6, A and B, and fig. S8, A to F). Unlabeled helper WBM cells were injected a day later to rescue from lethal busulfan conditioning (Fig. 6B). We hypothesized that there would be a cell population(s) that had higher capacity of CDMC engraftment than WBM control (which also contained the same population but in a much smaller number) in our BMT + P protocol. In this experiment, we specifically asked two questions: (i) Whether any of the eight hematopoietic cell types showed higher ability of CDMC engraftment than WBM before PLX5622 treatment and (ii) whether PLX5622 treatment for 10 days increased brain engraftment of CDMC derived from these hematopoietic cell types. We first analyzed the brain of the recipient mice at 4 weeks after transplantation before PLX5622 treatment (fig. S8A). We detected statistically significant GFP myeloid chimerism ($P < 0.05$) in the brain after transplantation of HSCs, common myeloid progenitors (CMPs), bone marrow monocytes, and WBM (Fig. 6C). Grafted HSCs resulted in by far the highest myeloid chimerism in the brain ranging from 10 to 40%. HSCs were the only population that showed higher capacity of CDMC engraftment than WBM at 4 weeks after transplantation. Moreover, HSC-derived CDMCs displayed already microglia-like ramified morphology unlike all other populations (fig. S9A).

We next sought to determine whether any of these four populations could give rise to high chimerism after PLX5622 treatment as seen with WBM. We therefore repeated the experiment with the four populations, this time using Kusabira orange–labeled helper WBM (Fig. 6D and fig. S9B) (*42*). Ten days after PLX5622 withdrawal, the HSC-derived CDMCs had almost completely outcompeted the helper WBM, unlike the other three populations (Fig. 6E). These results suggest that the brain incorporation activity is highly enriched in HSCs.

HSC-derived CDMCs and WBM-derived CDMCs had similar characteristics. The relative expression of CD45 and CD11b over time as measured by flow cytometry was comparable in the two populations (Fig. 6F). Both populations had a similar morphometric profile (Fig. 6, G and H). Just like WBM-CDMCs, HSC-derived CDMCs had higher expression of CD68 than microglia (Fig. 6, I and J). Last, RNA-seq analysis showed that HSC- and WBM-CDMCs clustered together in unsupervised hierarchical clustering and the PCA, respectively (Fig. 6K and fig. S9C). These results demonstrate that microglia can be efficiently replaced after transplantation with purified HSCs and HSC-derived CDMCs are morphologically and transcriptionally comparable to WBM-derived CDMCs.

Microglia replacement with CDMCs slows neurodegeneration, ameliorates motor dysfunction, and extends survival in Prosaposin-mutant mice

To assess the proof of concept that microglia replacement with CDMCs has therapeutic activity in the brain, we chose a genetic mouse model of a progressive neurodegenerative condition. The model contains three different genetic elements (*43*, *44*): (i) a homozygous D409H mutation in the *Gba1* gene ($Gba1^{D409H}$) encoding a lysosomal enzyme glucocerebrosidase (GCase); (ii) a homozygous knockout of Prosaposin (*Psap*), which is a known cofactor of GCase; and (iii) a *Psap* transgene (termed PS-NA), which renders overall PSAP protein quantity below 50%. Among other potential mechanisms, the mutant $Gba1^{D409H}$ and reduced PSAP protein in this mouse model cause reduced activity of GCase and accumulations of GCase substrates in tissues, and show a progressive neurodegenerative phenotype with loss of cerebellar Purkinje cells, astrogliosis, and behavioral cerebellar symptoms including progressive ataxia, waddle gait, and decreased life span (*43*). The pathology is primarily driven by reduced PSAP protein because homozygous $Gba1^{D409H}$ mice have only subtle phenotypes (*43*, *45*).

To allow syngeneic transplantation, we used littermates as donor mice. Littermate donors available were $Gba1^{D409/D409H}$; *Psap*-transgene; $Psap^{-/-}$ ($PSAP^{Low}$) or $Gba1^{D409/D409H}$; *Psap*-transgene; $Psap^{+/+}$ ($PSAP^{High}$) (Fig. 7A). Transplanted animals were compared to unmanipulated $PSAP^{Low}$ and $PSAP^{High}$ mice (Fig. 7B). We did not include a conventional BMT as control because brain chimerism is highly variable in this procedure (Fig. 1C), and therefore, results would be inconclusive. As opposed to testing disease prevention, we decided to evaluate microglia replacement with CDMCs at the young adolescent stage of ~8 to 9 weeks, at the time of disease symptoms initiation (*46*). After confirming successful peripheral blood and brain chimerism in this mouse strain using a Y chromosome–specific droplet digital PCR (fig. S10, A to C), we first analyzed protein expression of PSAP in the four different conditions at age 15 weeks (6 weeks after microglia replacement). We chose this time point for analyses of the brain because this mouse model at age 15 weeks shows motor dysfunction and accumulations of the GCase substrates, glucosylceramide (GC) and glucosylsphingosine, yet has several months to survive before premature death (*43*, *47*). PSAP immunofluorescence analysis in the cerebellum showed that PSAP protein expression was greatly reduced in $PSAP^{Low}$ mice and increased in both transplant groups (Fig. 7C). However, most of the PSAP signal in $PSAP^{Low}$ and $PSAP^{High}$ mice was located in Iba-1–negative compartments, whereas in the transplant groups PSAP was mostly overlapping with Iba-1 (Fig. 7C). Assuming that primarily the microglia-secreted PSAP may be therapeutic, we quantified PSAP expression inside ($Iba\text{-}1^{+}$) and outside ($Iba\text{-}1^{-}$) microglia separately. These results showed that secreted PSAP was elevated in both treatment groups, albeit not to quantity seen in $PSAP^{High}$ mice (Fig. 7D, left). PSAP staining within $Iba\text{-}1^{+}$ cells was elevated in both transplant groups, demonstrating that CDMCs have higher expression of PSAP from the *Psap* transgene than microglia (Fig. 7D, right). As expected, $PSAP^{High}$ CDMCs in $PSAP^{High}$→$PSAP^{Low}$ mice showed higher expression of PSAP protein than $PSAP^{Low}$ CDMCs in $PSAP^{Low}$→$PSAP^{Low}$ mice. Quantitative Western blotting confirmed the overall increase of PSAP protein in the cerebellum of the two transplant groups over the quantity in $PSAP^{Low}$ mice (Fig. 7, E and F). Thus, although CDMCs had higher expression of the *Psap* transgene than microglia in this neurodegeneration model, they secrete a smaller fraction of PSAP than microglia into the extracellular space. Although PSAP expression was increased in the transplant groups, it was not restored to the quantity in $PSAP^{High}$ mice.

We then evaluated whether the elevated PSAP protein observed in the brain would be sufficient to cause therapeutic effects. In this mouse model, two GCase substrates, GC and glucosylsphingosine, accumulate in the brain (fig. S11, A and B). We found that the total amount of six GC species with a different fatty acid acyl chain

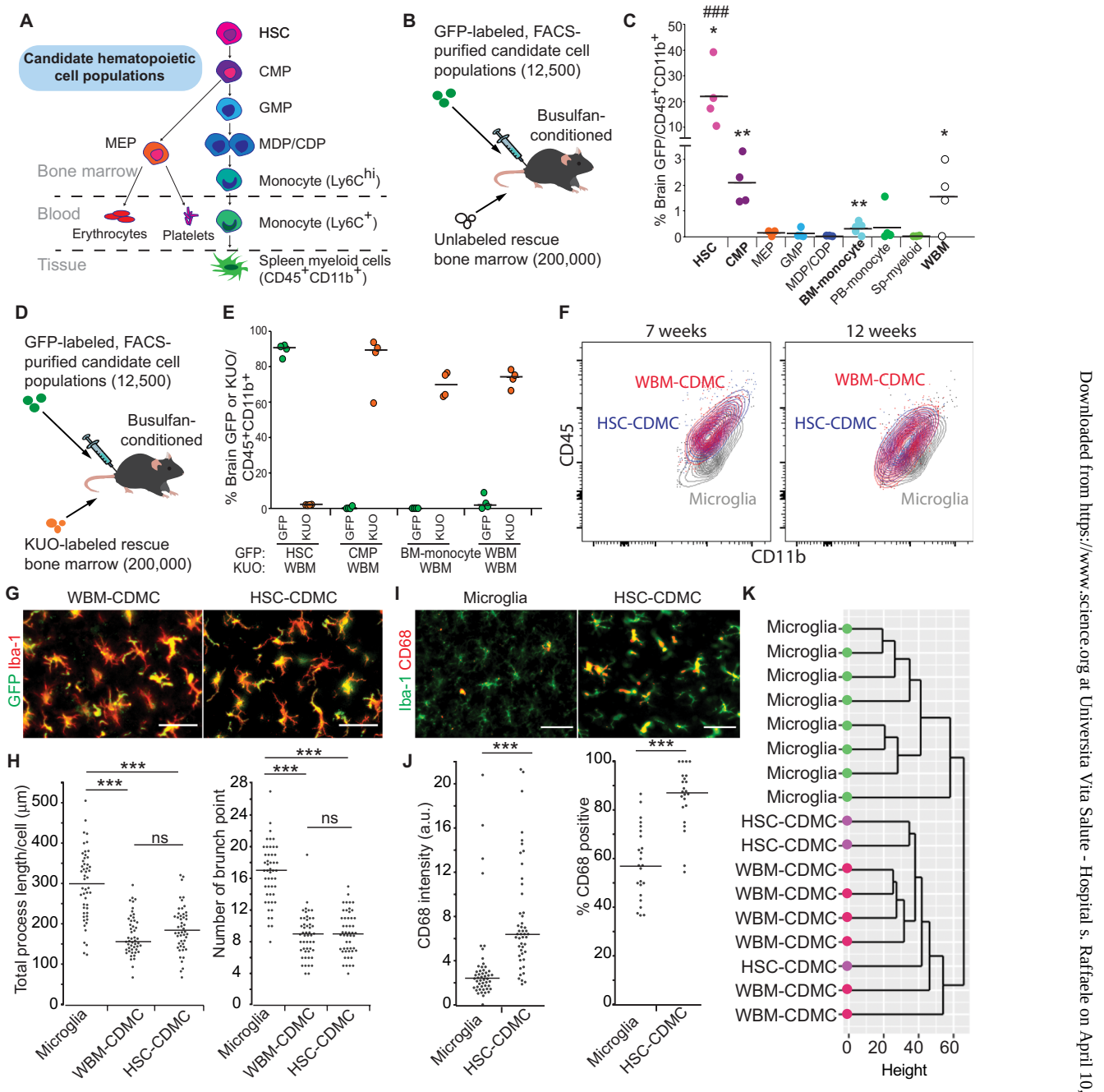

Fig. 6. Hematopoietic stem cells have the highest capacity to become brain CDMCs after BMT. (**A**) Schematic representation of the eight different hematopoietic subpopulations isolated for this experiment along with key surface markers used for sorting. HSC, hematopoietic stem cell; CMP, common myeloid progenitor; GMP, granulocyte/macrophage progenitor; MEP, megakaryocyte/erythrocyte progenitor; MDP/CDP, macrophage-dendritic progenitor/common dendritic progenitor. (**B**) Schematic of competitive transplantation using GFP-labeled hematopoietic populations (12.5×10^3 cells) and nonlabeled WBM (200×10^3 cells). (**C**) Percent GFP$^+$ cells among the brain's CD45$^+$CD11b$^+$ cell population were analyzed by flow cytometry on day 28. Sp, spleen (horizontal bars represent median values, $n = 4$ per population; $^*P < 0.05$ and $^{**}P < 0.01$; P values were calculated using a one-sample t test versus hypothetical value of 0; $^{\#\#\#}P < 0.001$ versus WBM, ANOVA). (**D**) Schematic of competitive transplantation using GFP-labeled hematopoietic populations (12.5×10^3 cells) and Kusabira orange (KUO)–labeled competitor cells (200×10^3 cells). (**E**) Percent GFP$^+$ cells and KUO$^+$ cells among the brain's CD45$^+$CD11b$^+$ cell population were analyzed by flow cytometry on day 48 (horizontal bars represent median values, $n = 4$ per population). (**F**) Overlaid density plots of WBM-CDMCs (red), HSC-CDMCs (blue), and microglia (gray) at the indicated time points. (**G**) Representative pictures of GFP$^+$ and Iba-1$^+$ cells in the cortex of WBM-transplanted mice (left) and HSC-transplanted mice (right). Scale bars, 50 μm. (**H**) Quantitative, morphological analysis of Iba-1$^+$ in the indicated samples. Left: Total length of processes. Right: Number of branch points (horizontal bars represent median values, $n = 3$ per group, three brain slices per animal were quantified; $^{***}P < 0.001$, ANOVA). (**I**) Immunofluorescence staining for Iba-1 and the activated microglia marker CD68 in untransplanted mice (microglia) and HSC-transplanted (HSC-CDMC) mice on day 48. Representative images are shown. Scale bars, 50 μm. (**J**) Quantification of CD68$^+$ cells in the indicated mice. Left: Fluorescence intensity of CD68. Right: Percentage of CD68$^+$ cells in Iba-1$^+$ cells (horizontal bars represent median values, $n = 3$ per group, three brain slices per animal; $^{***}P < 0.001$, Student's t test). a.u., arbitrary units. (**K**) Unsupervised hierarchical clustering of microglia, WBM-CDMCs, and HSC-CDMCs.

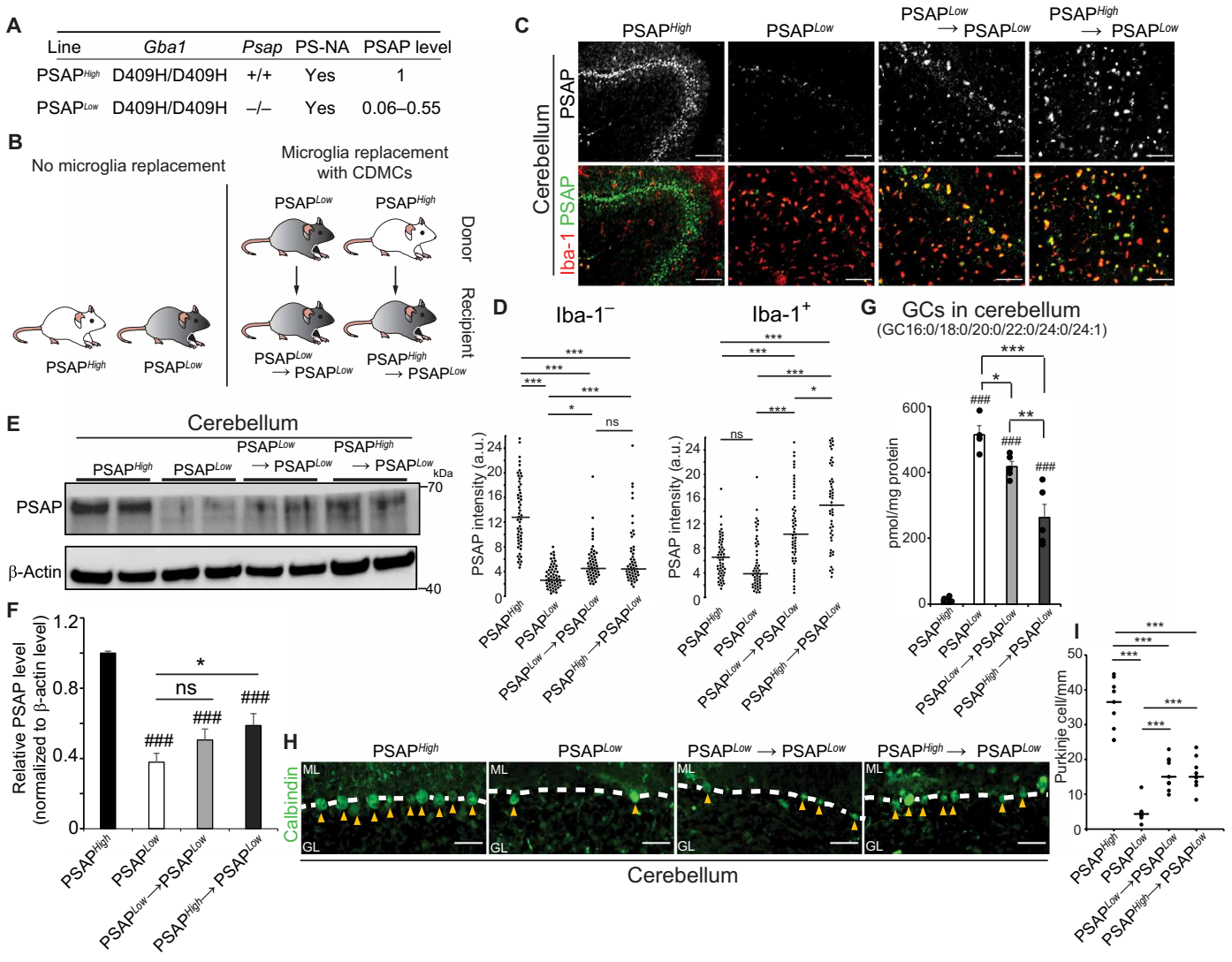

Fig. 7. Microglia replacement with CDMCs mitigates Purkinje cell degeneration in a mouse model of *Psap* deficiency. (**A**) Gene mutation and transgene in PSAP^{High} and PSAP^{Low} mice. PSAP^{Low} mice show symptoms of neurodegeneration. (**B**) Schematic of experimental BMT outline. (**C**) Representative pictures of PSAP^{+} and Iba-1^{+} cells in the cerebellum of indicated mice. Scale bars, 100 μm. (**D**) Quantitative analysis of fluorescence intensity of PSAP in Iba-1 compartment (left) and Iba-1^{+} cells (right) in the indicated samples (*$P < 0.05$ and ***$P < 0.001$, ANOVA). (**E**) Brain extracts from the cerebellum of the indicated groups were analyzed by Western blot for PSAP protein. Representative blot is shown. (**F**) Quantification of blots ($n = 6$ per group, $^{###}P < 0.001$ versus PSAP^{High}, *$P < 0.05$, ANOVA). (**G**) Six glucocerebrosidase (GC) species (GC16 : 0, GC18 : 0, GC20 : 0, GC22 : 0, GC24 : 0, and GC24 : 1) in the cerebellum of the indicated samples were quantified by supercritical fluid chromatography–tandem mass spectrometry ($n = 4$ to 5, $^{###}P < 0.001$ versus PSAP^{High}, *$P < 0.05$, **$P < 0.01$, and ***$P < 0.001$, ANOVA). (**H**) Representative pictures of calbindin-positive Purkinje cells (arrowheads) in the cerebellum in the indicated samples. ML, molecular layer; GL, granular layer. Scale bars, 50 μm. (**I**) Quantitative analysis of calbindin-positive Purkinje cells in the cerebellum of the indicated samples ($n = 3$ per group, three brain slices per animal were quantified; ***$P < 0.001$, ANOVA).

(GC16 : 0, GC18:0, GC20:0, GC22 : 0, GC24 : 0, and GC24:1) was significantly reduced ($P < 0.05$) in the cerebellum of PSAP^{Low}➔PSAP^{Low} and PSAP^{High}➔PSAP^{Low} mice compared to PSAP^{Low} mice (Fig. 7G). Glucosylsphingosine was not significantly reduced in the transplanted mice (fig. S11B, $P > 0.05$). One prominent feature of this model is progressive Purkinje cell degeneration and astrogliosis in thalamus and brain stem (*15*, *46*). Immunofluorescence microscopy and quantification at week 15 showed that more calbindin-positive Purkinje cells survived in the transplanted animals (Fig. 7, H and I) and astrogliosis was markedly reduced (fig. S12, A to D). Next, we performed behavioral assessments to assess cerebellar function such as balance, gait, and motor coordination. Reassuringly, both transplant groups showed improved performance in the beam walk test compared to PSAP^{Low} mice (Fig. 8, A and B). The fall score at 20 weeks was comparable between treated PSAP^{Low} mice and untreated PSAP^{High} mice; the time spent on the beam was significantly reduced in the treated mice (Fig. 8, A and B; $P < 0.001$). Gait coordination was assessed by footprint analysis (fig. S13, A and B). Again, both treatment groups showed an improvement of the ataxic gait that progresses in this mouse model (Fig. 8, C to F). Last, we examined general exploratory and locomotor activity in these mice by the open-field test. PSAP^{Low} mice showed an increase in Area Measure (a metric of the number of sharp turns instead of straight-line runs) over time, whereas no such increase was observed in treated mice

(Fig. 8G). In line with the behavioral improvements, the overall survival rate was improved in both treatment groups; $PSAP^{Low}$ mice transplanted with $PSAP^{High}$ cells survived significantly longer ($P = 0.01$) than untransplanted $PSAP^{Low}$ mice by 19.3%, and $PSAP^{Low}$ mice transplanted with $PSAP^{Low}$ donor cells trended to survive longer by 7.4% (Fig. 8H). The BMT + P procedure itself did not affect any of these behavioral parameters as $PSAP^{High}$➔$PSAP^{High}$ transplanted animals did not show any abnormalities (Fig. 8, A to G). In summary, these results demonstrate that high-efficiency microglia replacement with CDMCs by our BMT + P protocol increases PSAP protein in the brain, which leads to a therapeutic benefit in $PSAP^{Low}$ mice including a significant increase of survival ($P = 0.01$).

DISCUSSION

Finding therapeutic reagents that can cross the BBB remains challenging for treating neurological diseases. In this study, we show the proof of concept that a highly efficient microglia cell replacement with CDMCs provides therapeutic benefit in mice with a progressive neurodegenerative condition. This model combines mutant $Gba1^{D409H}$ and genetically reduced PSAP protein, which cause reduced GCase activity and GCase substrate accumulation and lead to pronounced CNS pathology (*43*, *44*). Because homozygous $Gba1^{D409H}$-mutant mice show only mild disease and the full *Psap* knockout is lethal, the primary genetic driver of the disease symptoms is the reduction of PSAP in this model (*43*). This is consistent with our observation that the phenotypes could be rescued by cells with higher PSAP secretion but still carrying the $Gba1^{D409H}$ mutation. Genetic *PSAP* deficiency in humans also causes various forms of progressive neurodegenerative conditions depending on the type of mutation in the *PSAP* gene (*48*–*51*). PSAP is a secreted protein that is taken up by surrounding cells and cleaved into saposins (A, B, C, and D) in the late endosome and lysosome, where they act as cofactors for lysosomal enzymes such as GCase (*52*–*54*). Consequently, we found GCase substrate reduction in transplanted animals carrying the $Gba1^{D409H}$ mutation, suggesting an increased GCase activity in vivo. A previous study showed that, unlike peripheral delivery of GCase, engineered GCase with increased brain permeability did exhibit therapeutic effects in a related *Psap*/*Gba1* mouse model (*15*). Therefore, it is possible that increased GCase activity in the CNS contributes to the phenotypic rescue that we observed. Thus, CDMCs engineered to efficiently secrete GCase may also improve symptoms in this model. We demonstrate that microglia replacement with CDMCs was able to reduce CNS pathology even when performed at around the time of disease onset, a timing more clinically realistic than prospective treatment. The treatment was no cure, however, as the therapeutic effects were partial. As newborn screening programs for genetic diseases have become more prevalent (*55*), earlier treatment may become feasible with likely larger therapeutic effects. The finding that microglia replacement can rectify CNS pathology is highly relevant for neural regeneration and provides a blueprint for cell-based brain therapies that could be potentially applied to a large variety of neurological diseases. Microglia are at the epicenter of regulating the pathogenesis of many diseases including neurodegeneration, traumatic injury, autoimmune disease, vascular brain insults, inflammatory disease, and brain tumors (*31*).

Another insight from this study is that primary HSCs can be used as donor cells for high-efficiency microglia replacement. Using HSCs as donor cells has some practical advantages as they are well defined, can be expanded in culture by several hundred-fold (*56*), and can be genetically manipulated by efficient lentiviral gene transfer, allowing the ex vivo genetic engineering of donor cells to bestow transplanted cells with additional therapeutic properties. We envision that HSC-like cells or other hematopoietic cells with equivalent microglia repopulating properties will eventually be generatable from induced pluripotent stem cells, which can be derived from patients in an autologous fashion and are amenable to an even wider spectrum of genetic engineering including therapeutic gene targeting by homologous recombination (*57*). The combination of microglia replacement with genetic donor cell engineering represents a versatile approach to interfere with brain pathology.

One experimental arm, the transplantation of $PSAP^{Low}$ donor cells to $PSAP^{Low}$ mice, that we had expected to be a negative control, resulted to be therapeutic because the transplanted CDMCs had higher expression of the *Psap* transgene than endogenous microglia. These results demonstrate the intriguing possibility that, under certain conditions, even transplantation with unaltered mutant cells may increase therapeutic gene expression when the gene of interest is expressed in CDMCs higher than microglia. This scenario would be applicable for known hypomorphic mutations whose increased expression would be expected to be therapeutic. For this purpose, it is beneficial that CDMCs are transcriptionally distinct from microglia independent of their method of integration as we and others have shown (*24*, *28*).

There are several limitations in our study. Given that our efficient BMT + P protocol enables a near-complete replacement of microglia with CDMCs in the brain, the question arises whether the observed differences between CDMCs and microglia in the normal brain are of relevance for overall brain function (*30*). In particular, long-term effects of microglia replacement are now not well understood. To that end, a recent study found subtle changes in transcriptional, histological, and behavioral features of mice with high CDMC chimerism (*16*). It is further possible that CDMCs mount a different immune response to CNS pathology than microglia. However, at least after bacterial LPS injection in WT mice, CDMC-containing brains respond very similarly to normal brains. It is unknown whether CDMCs and microglia mediate immune responses in a similar manner or not in disease brains. The functional differences between CDMCs and microglia in the normal brain are an interesting scientific question but of little practical relevance because CDMC transplantation would only be done in disease states. Given that microglia are highly reactive to CNS pathology (*30*, *58*), the potential positive or negative effects of CDMCs will have to be tested in specific disease environments. For instance, CDMCs in the normal brain induce a regional astrocytic activation (*16*), whereas in our mouse model for *Psap* deficiency, CDMCs effectively reduced astrogliosis.

Another limitation of our study is that BMT has severe side effects including immunosuppression and chemotherapy-associated toxicity. Therefore, at this point, our microglia replacement approach by the BMT + P protocol could only be applied to aggressive life-threatening diseases such as severe metabolic disorders or high-grade glioma, conditions for which BMT or chemotherapy is already applied. Important next steps of this work will be the development of a safer microglia replacement strategy that avoids toxic preconditioning analogous to the recently developed antibody-based preconditioning for BMT (*59*, *60*).

In summary, this study highlights microglial cells as an effective cellular target for cell-based therapies for regenerative efforts to restore

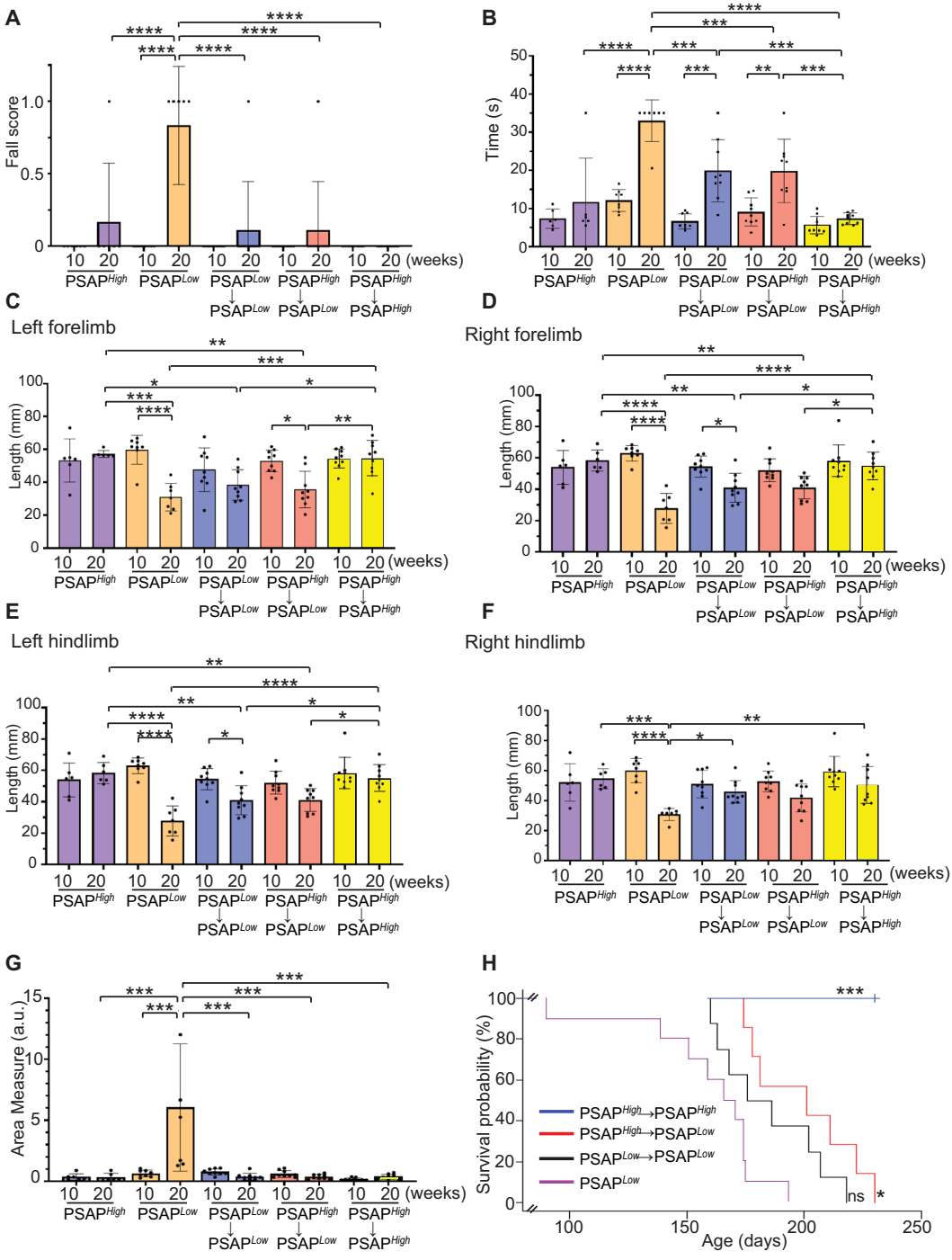

Fig. 8. Microglia replacement with CDMCs ameliorates disease progression in *Psap*-deficient mice. (**A** and **B**) Motor coordination in the indicated groups was evaluated by the elevated beam test. The beam used was 100 cm in length and 17 mm in width. Number of falling off the beam (A) (df = 9, $F = 8.377$, $P < 0.0001$) and time to cross the beam (B) (df = 9, $F = 18.33$, $P < 0.0001$) were measured. (**C** to **F**) Footprints of the indicated groups were evaluated for stride length of left forelimb (C) (df = 9, $F = 8.467$, $P < 0.0001$), right forelimb (D) (df = 9, $F = 12.47$, $P < 0.0001$), left hindlimb (E) (df = 9, $F = 6.486$, $P < 0.0001$), and right hindlimb (F) (df = 9, $F = 6.832$, $P < 0.0001$). (**G**) Locomotor behavior was assessed by the open-field test in the indicated groups. Plot demonstrates area measure, a metric of the number of sharp turns instead of straight-line runs during a 20-min open-field trial (df = 8, $F = 9.59$, $P < 0.0001$). All behavior assays were analyzed statistically by ANOVA. Mean ± SEM. *$P < 0.05$, **$P < 0.005$, ***$P < 0.0005$, and ****$P < 0.0001$. PSAP^{High} ($n = 6$), PSAP^{Low} ($n = 7$), PSAP^{Low}→PSAP^{Low} ($n = 9$), PSAP^{High}→PSAP^{Low} ($n = 9$), PSAP^{High}→PSAP^{High} ($n = 9$). (**H**) Life span of PSAP^{Low} (green, $n = 10$), PSAP^{Low}→PSAP^{Low} (black, $n = 9$), PSAP^{High}→PSAP^{Low} (red, $n = 7$), and PSAP^{High}→PSAP^{High} (blue, $n = 8$) (*$P < 0.05$ and ***$P < 0.001$ versus PSAP^{Low} mice, log rank; $\chi^2 = 35.9$, df = 3, $P < 0.0001$).

brain function. In combination with genetic engineering and the ability to transdifferentiate microglia into neural cells, microglia replacement will allow the efficient delivery of therapeutic agents into the brain and may even regenerate lost brain cells (*61*).

MATERIALS AND METHODS

Study design

The objectives of this study were to develop and characterize a BMT method that allows highly efficient replacement of microglia with donor CDMCs in mice and to evaluate therapeutic activity of microglia replacement in a mouse model of a neurodegenerative condition. We combined a conventional BMT protocol, based on chemotherapeutic bone marrow conditioning with busulfan, with the small-molecule inhibitor of CSF1R and achieved a near-complete and homogeneous replacement of microglia with donor CDMCs in C57BL/6 mice without the need for genetic manipulation of donor or host. To characterize CDMCs, RNA-seq and ex vivo phagocytosis assay were performed in isolated CDMCs and microglia. The brain bearing CDMCs was subjected to in vivo two-photon microscopy and morphological analysis. To evaluate the effects of CDMC incorporation on brain function, cytokine production analysis after LPS injection and the Y-maze spontaneous alternation test were performed in mice after our BMT method. To assess the proof of concept that microglia replacement has therapeutic activity in the brain, we performed our BMT method in a mouse model that shows

symptoms of neurodegeneration. Transplanted and untransplanted mice were subjected to behavioral tests including the open-field test, elevated beam test, and gait analysis. In addition, survival analysis was performed in those mice. The brain of the mice was subjected to immunofluorescence microscopy, Western blotting, and supercritical fluid chromatography–tandem mass spectrometry. All mice were randomized to different treatment groups. Replication and sample sizes for all experiments are described in the figure legends. No statistical methods were used to predetermine sample size. No data outliers were excluded. Investigators were blinded in the behavior tests and morphological analysis.

PLX5622 treatment

PLX5622 was provided by Plexxikon Inc. under a material transfer agreement and incorporated to AIN-76A standard chow by Research Diets Inc. at 1200 parts per million. Mice were treated with PLX5622 or control diet ad libitum for the duration indicated in the figure legends.

Bone marrow transplantation

Unless otherwise noted, we used female mice at age 8 to 12 weeks for both recipients and donors. WT mice were pretreated with PLX5622 diet between days −21 and −1 (21 days) and/or busulfan between days −6 and −2 (5 days). For busulfan pretreatment, mice received five intraperitoneal injections of busulfan (Sigma-Aldrich, B1170000) at 25 mg/kg body weight per day. On day 0, BMCs were isolated from tibias and femurs of UBC-GFP mice. Isolated BMCs were resuspended in 1× red blood cell lysis buffer (eBioscience, 00-4300-54) and incubated for 20 min at room temperature. BMCs were passed through a 70-μm cell strainer, washed by applying 10 ml of ice-cold PBS, and then resuspended in fresh PBS. BMCs (5×10^6) in 0.2 ml of PBS were injected into the retro-orbital sinus of the preconditioned recipients. On day 28, the recipient mice were treated with PLX5622 or control diet for 10 days. For tamoxifen injection, tamoxifen (Sigma-Aldrich, T5648) in corn oil (Sigma-Aldrich, C8267) was provided by intraperitoneal injection to the recipient mice at 200 mg/kg at the indicated time points after BMT.

Statistical analysis

In this study, *n* represents the number of animals used in experiments. For quantification in brain sections, we used at least three sections per animal. The number of brain sections used for quantification is presented in the figure legends. All bar graphs are mean values ± SEM. Statistical comparisons between two groups were made using unpaired, two-tailed, Student's *t* test. In Fig, 6C, a one-sample *t* test was used to compare mean values of the samples to the hypothetical value of 0. For group assessments, one-way analysis of variance (ANOVA) with post hoc analysis was performed. For survival analysis, the log-rank test was performed. All statistical analyses were performed either in R programming language or using GraphPad Prism.

SUPPLEMENTARY MATERIALS

www.science.org/doi/10.1126/scitranslmed.abl9945
Materials and Methods
Figs. S1 to S13
Table S1
Data file S1
Movies S1 and S2
References (*62*–*69*)

View/request a protocol for this paper from *Bio-protocol*.

REFERENCES AND NOTES

1. R. A. Barker, M. Parmar, L. Studer, J. Takahashi, Human trials of stem cell-derived dopamine neurons for Parkinson's disease: Dawn of a new era. *Cell Stem Cell* **21**, 569–573 (2017).
2. Y. Tao, S. C. Vermilyea, M. Zammit, J. Lu, M. Olsen, J. M. Metzger, L. Yao, Y. Chen, S. Phillips, J. E. Holden, V. Bondarenko, W. F. Block, T. E. Barnhart, N. Schultz-Darken, K. Brunner, H. Simmons, B. T. Christian, M. E. Emborg, S.-C. Zhang, Autologous transplant therapy alleviates motor and depressive behaviors in parkinsonian monkeys. *Nat. Med.* **27**, 632–639 (2021).
3. N. Gupta, R. G. Henry, J. Strober, S.-M. Kang, D. A. Lim, M. Bucci, E. Caverzasi, L. Gaetano, M. L. Mandelli, T. Ryan, R. Perry, J. Farrell, R. J. Jeremy, M. Ulman, S. L. Huhn, A. J. Barkovich, D. H. Rowitch, Neural stem cell engraftment and myelination in the human brain. *Sci. Transl. Med.* **4**, 155ra137 (2012).
4. E. A. Copelan, Hematopoietic stem-cell transplantation. *N. Engl. J. Med.* **354**, 1813–1826 (2006).
5. J. J. Malatack, D. M. Consolini, E. Bayever, The status of hematopoietic stem cell transplantation in lysosomal storage disease. *Pediatr. Neurol.* **29**, 391–403 (2003).
6. J. J. Boelens, V. K. Prasad, J. Tolar, R. F. Wynn, C. Peters, Current international perspectives on hematopoietic stem cell transplantation for inherited metabolic disorders. *Pediatr. Clin. North Am.* **57**, 123–145 (2010).
7. J. M. Rappeport, E. I. Ginns, Bone-marrow transplantation in severe Gaucher's disease. *N. Engl. J. Med.* **311**, 84–88 (1984).
8. O. Ringdén, C. G. Groth, A. Erikson, L. Bäckman, S. Granqvist, J. E. Månsson, L. Svennerholm, Long-term follow-up of the first successful bone marrow transplantation in Gaucher disease. *Transplantation* **46**, 66–69 (1988).
9. B. Ajami, J. L. Bennett, C. Krieger, W. Tetzlaff, F. M. V. Rossi, Local self-renewal can sustain CNS microglia maintenance and function throughout adult life. *Nat. Neurosci.* **10**, 1538–1543 (2007).
10. F. Ginhoux, M. Greter, M. Leboeuf, S. Nandi, P. See, S. Gokhan, M. F. Mehler, S. J. Conway, L. G. Ng, E. R. Stanley, I. M. Samokhvalov, M. Merad, Fate mapping analysis reveals that adult microglia derive from primitive macrophages. *Science* **330**, 841–845 (2010).
11. M. R. P. Elmore, A. R. Najafi, M. A. Koike, N. N. Dagher, E. E. Spangenberg, R. A. Rice, M. Kitazawa, B. Matusow, H. Nguyen, B. L. West, K. N. Green, Colony-stimulating factor 1 receptor signaling is necessary for microglia viability, unmasking a microglia progenitor cell in the adult brain. *Neuron* **82**, 380–397 (2014).
12. E. Gomez Perdiguero, K. Klapproth, C. Schulz, K. Busch, E. Azzoni, L. Crozet, H. Garner, C. Trouillet, M. F. de Bruijn, F. Geissmann, H.-R. Rodewald, Tissue-resident macrophages originate from yolk-sac-derived erythro-myeloid progenitors. *Nature* **518**, 547–551 (2015).
13. P. Füger, J. K. Hefendehl, K. Veeraraghavalu, A.-C. Wendeln, C. Schlosser, U. Obermüller, B. M. Wegenast-Braun, J. J. Neher, P. Martus, S. Kohsaka, M. Thunemann, R. Feil, S. S. Sisodia, A. Skodras, M. Jucker, Microglia turnover with aging and in an Alzheimer's model via long-term in vivo single-cell imaging. *Nat. Neurosci.* **20**, 1371–1376 (2017).
14. M. F. Coutinho, J. I. Santos, S. Alves, Less is more: Substrate reduction therapy for lysosomal storage disorders. *Int. J. Mol. Sci.* **17**, 1065 (2016).
15. Y. Sun, B. Liou, Z. Chu, V. Fannin, R. Blackwood, Y. Peng, G. A. Grabowski, H. W. Davis, X. Qi, Systemic enzyme delivery by blood-brain barrier-penetrating SapC-DOPS nanovesicles for treatment of neuronopathic Gaucher disease. *EBioMedicine* **55**, 102735 (2020).
16. L. A. Hohsfield, A. R. Najafi, Y. Ghorbanian, N. Soni, E. E. Hingco, S. J. Kim, A. D. Jue, V. Swarup, M. A. Inlay, K. N. Green, Effects of long-term and brain-wide colonization of peripheral bone marrow-derived myeloid cells in the CNS. *J. Neuroinflammation* **17**, –279 (2020).
17. Z. Xu, Y. Rao, Y. Huang, T. Zhou, R. Feng, S. Xiong, T.-F. Yuan, S. Qin, Y. Lu, X. Zhou, X. Li, B. Qin, Y. Mao, B. Peng, Efficient strategies for microglia replacement in the central nervous system. *Cell Rep.* **32**, 108041 (2020).
18. A. Capotondo, R. Milazzo, L. S. Politi, A. Quattrini, A. Palini, T. Plati, S. Merella, A. Nonis, C. di Serio, E. Montini, L. Naldini, A. Biffi, Brain conditioning is instrumental for successful microglia reconstitution following hematopoietic stem cell transplantation. *Proc. Natl. Acad. Sci. U.S.A.* **109**, 15018–15023 (2012).
19. A. Lampron, M. Lessard, S. Rivest, Effects of myeloablation, peripheral chimerism, and whole-body irradiation on the entry of bone marrow-derived cells into the brain. *Cell Transplant.* **21**, 1149–1159 (2012).
20. A. Shemer, J. Grozovski, T. L. Tay, J. Tao, A. Volaski, P. Süß, A. Ardura-Fabregat, M. Gross-Vered, J.-S. Kim, E. David, L. Chappell-Maor, L. Thielecke, C. K. Glass, K. Cornils, M. Prinz, S. Jung, Engrafted parenchymal brain macrophages differ from microglia in transcriptome, chromatin landscape and response to challenge. *Nat. Commun.* **9**, 5206 (2018).
21. F. L. Wilkinson, A. Sergijenko, K. J. Langford-Smith, M. Malinowska, R. F. Wynn, B. W. Bigger, Busulfan conditioning enhances engraftment of hematopoietic donor-derived cells in the brain compared with irradiation. *Mol. Ther.* **21**, 868–876 (2013).

22. A. S. Youshani, S. Rowlston, C. O'Leary, G. Forte, H. Parker, A. Liao, B. Telfer, K. Williams, I. D. Kamaly-Asl, B. W. Bigger, Non-myeloablative busulfan chimeric mouse models are less pro-inflammatory than head-shielded irradiation for studying immune cell interactions in brain tumours. *J. Neuroinflammation* **16**, 25 (2019).
23. J. Priller, A. Flügel, T. Wehner, M. Boentert, C. A. Haas, M. Prinz, F. Fernández-Klett, K. Prass, I. Bechmann, B. A. de Boer, M. Frotscher, G. W. Kreutzberg, D. A. Persons, U. Dirnagl, Targeting gene-modified hematopoietic cells to the central nervous system: Use of green fluorescent protein uncovers microglial engraftment. *Nat. Med.* **7**, 1356–1361 (2001).
24. F. C. Bennett, M. L. Bennett, F. Yaqoob, S. B. Mulinyawe, G. A. Grant, M. Hayden Gephart, E. D. Plowey, B. A. Barres, A combination of ontogeny and CNS environment establishes microglial identity. *Neuron* **98**, 1170–1183.e8 (2018).
25. Y. Huang, Z. Xu, S. Xiong, F. Sun, G. Qin, G. Hu, J. Wang, L. Zhao, Y.-X. Liang, T. Wu, Z. Lu, M. S. Humayun, K.-F. So, Y. Pan, N. Li, T.-F. Yuan, Y. Rao, B. Peng, Repopulated microglia are solely derived from the proliferation of residual microglia after acute depletion. *Nat. Neurosci.* **21**, 530–540 (2018).
26. N. N. Dagher, A. R. Najafi, K. M. N. Kayala, M. R. P. Elmore, T. E. White, R. Medeiros, B. L. West, K. N. Green, Colony-stimulating factor 1 receptor inhibition prevents microglial plaque association and improves cognition in 3xTg-AD mice. *J. Neuroinflammation* **12**, 139 (2015).
27. M. Valdearcos, J. D. Douglass, M. M. Robblee, M. D. Dorfman, D. R. Stifler, M. L. Bennett, I. Gerritse, R. Fasnacht, B. A. Barres, J. P. Thaler, S. K. Koliwad, Microglial inflammatory signaling orchestrates the hypothalamic immune response to dietary excess and mediates obesity susceptibility. *Cell Metab.* **26**, 185–197.e3 (2017).
28. J. C. Cronk, A. J. Filiano, A. Louveau, I. Marin, R. Marsh, E. Ji, D. H. Goldman, I. Smirnov, N. Geraci, S. Acton, C. C. Overall, J. Kipnis, Peripherally derived macrophages can engraft the brain independent of irradiation and maintain an identity distinct from microglia. *J. Exp. Med.* **215**, 1627–1647 (2018).
29. H. Lund, M. Pieber, R. Parsa, J. Han, D. Grommisch, E. Ewing, L. Kular, M. Needhamsen, A. Espinosa, E. Nilsson, A. K. Överby, O. Butovsky, M. Jagodic, X.-M. Zhang, R. A. Harris, Competitive repopulation of an empty microglial niche yields functionally distinct subsets of microglia-like cells. *Nat. Commun.* **9**, 4845 (2018).
30. Q. Li, B. A. Barres, Microglia and macrophages in brain homeostasis and disease. *Nat. Rev. Immunol.* **18**, 225–242 (2018).
31. M. W. Salter, B. Stevens, Microglia emerge as central players in brain disease. *Nat. Med.* **23**, 1018–1027 (2017).
32. H. Keren-Shaul, A. Spinrad, A. Weiner, O. Matcovitch-Natan, R. Dvir-Szternfeld, T. K. Ulland, E. David, K. Baruch, D. Lara-Astaiso, B. Toth, S. Itzkovitz, M. Colonna, M. Schwartz, I. Amit, A unique microglia type associated with restricting development of Alzheimer's disease. *Cell* **169**, 1276–1290.e17 (2017).
33. S. Krasemann, C. Madore, R. Cialic, C. Baufeld, N. Calcagno, R. El Fatimy, L. Beckers, E. O'Loughlin, Y. Xu, Z. Fanek, D. J. Greco, S. T. Smith, G. Tweet, Z. Humulock, T. Zrzavy, P. Conde-Sanroman, M. Gacias, Z. Weng, H. Chen, E. Tjon, F. Mazaheri, K. Hartmann, A. Madi, J. D. Ulrich, M. Glatzel, A. Worthmann, J. Heeren, B. Budnik, C. Lemere, T. Ikezu, F. L. Heppner, V. Litvak, D. M. Holtzman, H. Lassmann, H. L. Weiner, J. Ochando, C. Haass, O. Butovsky, The TREM2-APOE pathway drives the transcriptional phenotype of dysfunctional microglia in neurodegenerative diseases. *Immunity* **47**, 566–581.e9 (2017).
34. C. E. G. Leyns, J. D. Ulrich, M. B. Finn, F. R. Stewart, L. J. Koscal, J. R. Serrano, G. O. Robinson, E. Anderson, M. Colonna, D. M. Holtzman, TREM2 deficiency attenuates neuroinflammation and protects against neurodegeneration in a mouse model of tauopathy. *Proc. Natl. Acad. Sci. U.S.A.* **114**, 11524–11529 (2017).
35. M. Olah, E. Patrick, A.-C. Villani, J. Xu, C. C. White, K. J. Ryan, P. Piehowski, A. Kapasi, P. Nejad, M. Cimpean, S. Connor, C. J. Yung, M. Frangieh, A. McHenry, W. Elyaman, V. Petyuk, J. A. Schneider, D. A. Bennett, P. L. De Jager, E. M. Bradshaw, A transcriptomic atlas of aged human microglia. *Nat. Commun.* **9**, 539 (2018).
36. M. L. Bennett, F. C. Bennett, S. A. Liddelow, B. Ajami, J. L. Zamanian, N. B. Fernhoff, S. B. Mulinyawe, C. J. Bohlen, A. Adil, A. Tucker, I. L. Weissman, E. F. Chang, G. Li, G. A. Grant, M. G. Hayden Gephart, B. A. Barres, New tools for studying microglia in the mouse and human CNS. *Proc. Natl. Acad. Sci. U.S.A.* **113**, E1738–E1746 (2016).
37. K. I. Mosher, T. Wyss-Coray, Microglial dysfunction in brain aging and Alzheimer's disease. *Biochem. Pharmacol.* **88**, 594–604 (2014).
38. D. Davalos, J. Grutzendler, G. Yang, J. V. Kim, Y. Zuo, S. Jung, D. R. Littman, M. L. Dustin, W.-B. Gan, ATP mediates rapid microglial response to local brain injury in vivo. *Nat. Neurosci.* **8**, 752–758 (2005).
39. A. Nimmerjahn, F. Kirchhoff, F. Helmchen, Resting microglial cells are highly dynamic surveillants of brain parenchyma in vivo. *Science* **308**, 1314–1318 (2005).
40. T. Goldmann, P. Wieghofer, P. F. Müller, Y. Wolf, D. Varol, S. Yona, S. M. Brendecke, K. Kierdorf, O. Staszewski, M. Datta, T. Luedde, M. Heikenwalder, S. Jung, M. Prinz, A new type of microglia gene targeting shows TAK1 to be pivotal in CNS autoimmune inflammation. *Nat. Neurosci.* **16**, 1618–1626 (2013).
41. J. Seita, I. L. Weissman, Hematopoietic stem cell: Self-renewal versus differentiation. *Wiley Interdiscip. Rev. Syst. Biol. Med.* **2**, 640–653 (2010).
42. S. Hamanaka, J. Ooehara, Y. Morita, H. Ema, S. Takahashi, A. Miyawaki, M. Otsu, T. Yamaguchi, M. Onodera, H. Nakauchi, Generation of transgenic mouse line expressing Kusabira Orange throughout body, including erythrocytes, by random segregation of provirus method. *Biochem. Biophys. Res. Commun.* **435**, 586–591 (2013).
43. Y. Sun, B. Quinn, D. P. Witte, G. A. Grabowski, Gaucher disease mouse models: Point mutations at the acid β-glucosidase locus combined with low-level prosaposin expression lead to disease variants. *J. Lipid Res.* **46**, 2102–2113 (2005).
44. V. Schiffer, E. Santiago-Mujika, S. Flunkert, S. Schmidt, M. Farcher, T. Loeffler, I. Schilcher, M. Posch, J. Neddens, Y. Sun, J. Kehr, B. Hutter-Paier, Characterization of the visceral and neuronal phenotype of 4L/PS-NA mice modeling Gaucher disease. *PLOS ONE* **15**, e0227077 (2020).
45. Y.-H. Xu, B. Quinn, D. Witte, G. A. Grabowski, Viable mouse models of acid beta-glucosidase deficiency: The defect in Gaucher disease. *Am. J. Pathol.* **163**, 2093–2101 (2003).
46. Y. Sun, L. Jia, M. T. Williams, M. Zamzow, H. Ran, B. Quinn, B. J. Aronow, C. V. Vorhees, D. P. Witte, G. A. Grabowski, Temporal gene expression profiling reveals CEBPD as a candidate regulator of brain disease in prosaposin deficient mice. *BMC Neurosci.* **9**, 76 (2008).
47. Y. Sun, W. Zhang, Y.-H. Xu, B. Quinn, N. Dasgupta, B. Liou, K. D. R. Setchell, G. A. Grabowski, Substrate compositional variation with tissue/region and Gba1 mutations in mouse models–implications for Gaucher disease. *PLOS ONE* **8**, e57560 (2013).
48. L. Calderwood, D. A. Wenger, D. Matern, H. Dahmoush, V. Watiker, C. Lee, Rare Saposin A deficiency: Novel variant and psychosine analysis. *Mol. Genet. Metab.* **129**, 161–164 (2020).
49. R. Spiegel, G. Bach, V. Sury, G. Mengistu, B. Meidan, S. Shalev, Y. Shneor, H. Mandel, M. Zeigler, A mutation in the saposin A coding region of the prosaposin gene in an infant presenting as Krabbe disease: First report of saposin A deficiency in humans. *Mol. Genet. Metab.* **84**, 160–166 (2005).
50. A. Diaz-Font, B. Cormand, R. Santamaria, L. Vilageliu, D. Grinberg, A. Chabás, A mutation within the saposin D domain in a Gaucher disease patient with normal glucocerebrosidase activity. *Hum. Genet.* **117**, 275–277 (2005).
51. M. Cesani, L. Lorioli, S. Grossi, G. Amico, F. Fumagalli, I. Spiga, M. Filocamo, A. Biffi, Mutation update of ARSA and PSAP genes causing metachromatic leukodystrophy. *Hum. Mutat.* **37**, 16–27 (2016).
52. M. Hiraiwa, B. M. Martin, Y. Kishimoto, G. E. Conner, S. Tsuji, J. S. O'Brien, Lysosomal proteolysis of prosaposin, the precursor of saposins (sphingolipid activator proteins)—Its mechanism and inhibition by ganglioside. *Arch. Biochem. Biophys.* **341**, 17–24 (1997).
53. T. Leonova, X. Qi, A. Bencosme, E. Ponce, Y. Sun, G. A. Grabowski, Proteolytic processing patterns of prosaposin in insect and mammalian cells. *J. Biol. Chem.* **271**, 17312–17320 (1996).
54. T. Hiesberger, S. Hüttler, A. Rohlmann, W. Schneider, K. Sandhoff, J. Herz, Cellular uptake of saposin (SAP) precursor and lysosomal delivery by the low density lipoprotein receptor-related protein (LRP). *EMBO J.* **17**, 4617–4625 (1998).
55. Z. I. Remec, K. Trebusak Podkrajsek, B. Repic Lampret, J. Kovac, U. Groselj, T. Tesovnik, T. Battelino, M. Debeljak, Next-generation sequencing in newborn screening: A review of current state. *Front. Genet.* **12**, 662254 (2021).
56. A. C. Wilkinson, R. Ishida, M. Kikuchi, K. Sudo, M. Morita, R. V. Crisostomo, R. Yamamoto, K. M. Loh, Y. Nakamura, M. Watanabe, H. Nakauchi, S. Yamazaki, Long-term ex vivo haematopoietic-stem-cell expansion allows nonconditioned transplantation. *Nature* **571**, 117–121 (2019).
57. J. Hanna, M. Wernig, S. Markoulaki, C.-W. Sun, A. Meissner, J. P. Cassady, C. Beard, T. Brambrink, L.-C. Wu, T. M. Townes, R. Jaenisch, Treatment of sickle cell anemia mouse model with iPS cells generated from autologous skin. *Science* **318**, 1920–1923 (2007).
58. E. B. Vitner, T. Farfel-Becker, R. Eilam, I. Biton, A. H. Futerman, Contribution of brain inflammation to neuronal cell death in neuronopathic forms of Gaucher's disease. *Brain* **135**, 1724–1735 (2012).
59. A. Chhabra, A. M. Ring, K. Weiskopf, P. J. Schnorr, S. Gordon, A. C. Le, H.-S. Kwon, N. G. Ring, J. Volkmer, P. Y. Ho, S. Tseng, I. L. Weissman, J. A. Shizuru, Hematopoietic stem cell transplantation in immunocompetent hosts without radiation or chemotherapy. *Sci. Transl. Med.* **8**, 351ra105 (2016).
60. B. M. George, K. S. Kao, H.-S. Kwon, B. J. Velasco, J. Poyser, A. Chen, A. C. Le, A. Chhabra, C. E. Burnett, D. Cajuste, M. Hoover, K. M. Loh, J. A. Shizuru, I. L. Weissman, Antibody conditioning enables MHC-mismatched hematopoietic stem cell transplants and organ graft tolerance. *Cell Stem Cell* **25**, 185–192.e3 (2019).
61. T. Matsuda, T. Irie, S. Katsurabayashi, Y. Hayashi, T. Nagai, N. Hamazaki, A. M. D. Adefuin, F. Miura, T. Ito, H. Kimura, K. Shirahige, T. Takeda, K. Iwasaki, T. Imamura, K. Nakashima, Pioneer factor NeuroD1 rearranges transcriptional and epigenetic profiles to execute microglia-neuron conversion. *Neuron* **101**, 472–485.e7 (2019).
62. Y. Shibuya, C. C. Y. Chang, L.-H. Huang, E. Y. Bryleva, T.-Y. Chang, Inhibiting ACAT1/SOAT1 in microglia stimulates autophagy-mediated lysosomal proteolysis and increases Aβ1–42 clearance. *J. Neurosci.* **34**, 14484–14501 (2014).
63. K. Young, H. Morrison, Quantifying microglia morphology from photomicrographs of immunohistochemistry prepared tissue using ImageJ. *J. Vis. Exp.* , e57648 (2018).

64. C. J. Henry, Y. Huang, A. Wynne, M. Hanke, J. Himler, M. T. Bailey, J. F. Sheridan, J. P. Godbout, Minocycline attenuates lipopolysaccharide (LPS)-induced neuroinflammation, sickness behavior, and anhedonia. *J. Neuroinflammation* **5**, 15 (2008).
65. M. A. Mohr, D. Bushey, A. Aggarwal, J. S. Marvin, J. J. Kim, E. J. Marquez, Y. Liang, R. Patel, J. J. Macklin, C.-Y. Lee, A. Tsang, G. Tsegaye, A. M. Ahrens, J. L. Chen, D. S. Kim, A. M. Wong, L. L. Looger, E. R. Schreiter, K. Podgorski, jYCaMP: An optimized calcium indicator for two-photon imaging at fiber laser wavelengths. *Nat. Methods* **17**, 694–697 (2020).
66. M. W. Pfaffl, G. W. Horgan, L. Dempfle, Relative expression software tool (REST©) for group-wise comparison and statistical analysis of relative expression results in real-time PCR. *Nucleic Acids Res.* **30**, e36 (2002).
67. R. Yamamoto, A. C. Wilkinson, J. Ooehara, X. Lan, C.-Y. Lai, Y. Nakauchi, J. K. Pritchard, H. Nakauchi, Large-scale clonal analysis resolves aging of the mouse hematopoietic stem cell compartment. *Cell Stem Cell* **22**, 600–607.e4 (2018).
68. M. Faizi, P. L. Bader, N. Saw, T.-V. V. Nguyen, S. Beraki, T. Wyss-Coray, F. M. Longo, M. Shamloo, Thy1-hAPP$^{Lond/Swe+}$ mouse model of Alzheimer's disease displays broad behavioral deficits in sensorimotor, cognitive and social function. *Brain Behav.* **2**, 142–154 (2012).
69. S. C. Fowler, B. R. Birkestrand, R. Chen, S. J. Moss, E. Vorontsova, G. Wang, T. J. Zarcone, A force-plate actometer for quantitating rodent behaviors: Illustrative data on locomotion, rotation, spatial patterning, stereotypies, and tremor. *J. Neurosci. Methods* **107**, 107–124 (2001).

Acknowledgments: We would like to thank all members of the Wernig laboratory, J. Pluvinage, D. Mochly-Rosen, and K. Grimes for helpful discussions throughout the project and T. Broer, M. R. Casilla, FACS core at Institute for Stem Cell Biology and Regenerative Medicine, and Stanford Neuroscience Microscopy Service (supported by NIH NS069375) for technical support. **Funding:** The project was supported by a pilot grant from the Stanford Alzheimer's Disease Research Center NIH grant (P50AG047366 to M.W.), Howard Hughes Medical Institute Faculty Scholar Award, and the Goldman-Sachs Foundation to M.W. Y. Shibuya was supported by the Larry L. Hillblom Foundation Postdoctoral Fellowship (2017-A-016-FEL). K.K.K. was supported by the Stanford Neurosurgery Resident Research Education Program R25 (NIH NS065741-10). M.M.-D.M. was supported by Deutsche Forschungsgemeinschaft (DFG) (MA 8492/1-1). Y.Y. was supported by the New York Stem Cell Foundation Druckenmiller Fellowship (NYSCF–D–F74). L.A.A. was supported by grants from the NIH and California Institute of Regenerative Medicine (CIRM) awarded to L.A.A.'s home institution, San Francisco State University (R25-GM059298, CIRM:EDUC2-08391). **Author contributions:** Study concept and design: Y. Shibuya and M.W. BMT and posttransplantation analyses: Y. Shibuya, K.K.K., M.M.-D.M., Y.Y., L.A.A., I.K., R.Y., and P.M. RNA-seq data processing: Y.Y. Two-photon microscopy: M.M.-D.M. and M.A.M. Droplet digital PCR: G.N. Behavioral tests: K.K.K. and M.Z. Development and maintenance of *Psap*-deficient mice: B.L. and Y. Sun. Supervision and suggestions on data interpretation: T.C.S., T.W.-C., F.L.H., X.C., Y. Sun, H.N., and F.C.B. Drafting of original manuscript: Y. Shibuya and M.W. All authors reviewed, revised, and approved the final version of the paper. **Competing interests:** The authors declare that they have no competing interests. **Data and materials availability:** All data associated with this study are present in the paper or the Supplementary Materials. The bulk RNA-seq dataset generated in this study is available at the NCBI BioProject (www.ncbi.nlm.nih.gov/bioproject), accession no: PRJNA600501. PLX5622 was provided by Plexxikon Inc. under a material transfer agreement between Stanford University and Plexxikon Inc.

Submitted 19 August 2021
Resubmitted 27 January 2022
Accepted 10 February 2022
Published 16 March 2022
10.1126/scitranslmed.abl9945

Science Translational Medicine

Treatment of a genetic brain disease by CNS-wide microglia replacement

Yohei ShibuyaKevin K. KumarMarius Marc-Daniel MaderYongjin YooLuis Angel AyalaMu ZhouManuel Alexander MohrGernot NeumayerIshan KumarRyo YamamotoPaul MarcouxBenjamin LiouF. Chris BennettHiromitsu NakauchiYing SunXiaoke ChenFrank L. HeppnerTony Wyss-CorayThomas C. SüdhofMarius Wernig

Sci. Transl. Med., 14 (636), eabl9945. • DOI: 10.1126/scitranslmed.abl9945

Efficient replacement

Cell therapies have the potential of being an effective approach for treating neurodegenerative conditions. However, the need for local delivery and the poor distribution of the transplanted cells hinder the development of effective treatments. Here, Shibuya *et al.* developed an efficient microglia replacement approach in rodents using circulation-derived myeloid cells (CDMCs). The cells broadly incorporated in the brain and generated microglia-like cells more efficiently than bone marrow transplant. In a mouse model of progressive neurodegeneration, CDMC-mediated microglia replacement reduced cell loss and brain inflammation, improved motor behavior, and extended life span. The results suggest that this approach might be therapeutic in multiple neurological conditions.

Science Translational Medicine (ISSN) is published by the American Association for the Advancement of Science. 1200 New York Avenue NW, Washington, DC 20005. The title *Science Translational Medicine* is a registered trademark of AAAS.